Reports on Progress in **Physics**

REVIEW • **OPEN ACCESS**

Review on band structure and spin polarization of altermagnetic materials

To cite this article: Xiangnan Xie *et al* 2026 *Rep. Prog. Phys.* **89** 076504

IOP Publishing Rep. Prog. Phys. 89 (2026) 076504 https://doi.org/10.1088/1361-6633/ae8868

Reports on Progress in Physics

OPEN ACCESS

RECEIVED
18 January 2026

REVISED
29 March 2026

ACCEPTED FOR PUBLICATION
9 July 2026

PUBLISHED
28 July 2026

REVIEW

Review on band structure and spin polarization of altermagnetic materials

Xiangnan Xie[1,4], **Xiaoyue He**[2,4], **Fayuan Zhang**[3,4] **and Chaoyu Chen**[2,*]

[1] College of Science, National University of Defense Technology, Changsha 410073, People's Republic of China
[2] Songshan Lake Materials Laboratory, Dongguan 523808, People's Republic of China
[3] Quantum Science Center of Guangdong–Hong Kong–Macao Greater Bay Area (Guangdong), Shenzhen 518045, People's Republic of China
[4] These authors contributed equally to this work.
[*] Author to whom any correspondence should be addressed.

E-mail: chenchaoyu@sslab.org.cn

Keywords: altermagnet, spin splitting, spin polarization, ARPES, spin–momentum locking

Corresponding editor: Dr Mei-Yin Chou

Abstract

Recent theoretical and experimental efforts have revealed the existence of a new class of magnetic materials, altermagnets, characterized by distinct symmetries in spin and real space. Combining the properties of ferromagnets, such as band spin polarization and time-reversal symmetry breaking responses, and antiferromagnets, like vanishing stray field and terahertz magnon dynamics, altermagnets are attracting enormous attention in both magnetism and spintronics community. While numerous altermagnetic candidates and emerging physical properties have been studied in theory extensively and enthusiastically, the experimental investigation of altermagnetism is struggling against the lack of proper altermagnetic materials and the controversial results reported for specific candidates. In this review, we first give a general description on the concept and key properties of altermagnetism, outline its distinction from other compensated magnetic order from the aspects of time-reversal symmetry in the spin momentum locking texture and time-reversal symmetry breaking responses. The main body of this review concentrates on the progress in altermagnetic material study with special focus on their band structure and spin polarization features, as well as the controversies over several candidate materials. Going forward, we point out several directions which altermagnetic material investigation might follow and guidelines which could help to avoid the pitfalls in the experimental pursuit of ideal altermagnets.

1. Introduction

In the past four years, we have witnessed the explosive increase of altermagnet related fundamental researches ranging from theoretical calculation [1–154], material synthesis [155–169], structure and magnetic structure [170–182], to band structure and spin polarization study [183–202]. The unique combination of ferromagnetic and antiferromagnetic properties in altermagnets places this novel state of matter at the frontier of magnetism and spintronics study. The distinct symmetries in spin and lattice space of altermagnets [16, 17] lead to band spin polarization [1, 2, 4–6, 8, 10, 17], unconventional spin splitting effects and spin currents [3, 7, 203–211], unconventional piezomagnetism [8, 34, 57, 77, 212] as well as the possibility of various time-reversal symmetry (T-symmetry) breaking responses including x-ray magnetic linear/circular dichroism (XMCD) [103, 213–223], anomalous Hall effect (AHE) [1, 65, 124, 224–235], magneto-optical Kerr effect (MOKE) [82, 106, 236, 237], orientation-dependent giant/-tunneling magnetoresistance (GMR/TMR) [14, 23, 43, 238–240] and their thermal [241–245] and magnonic [29, 94, 143, 246–250] counterparts. Furthermore, the compatibility of altermagnets with other spontaneous quantum orders in the same material enables the interplay of altermagnetism with exotic phenomena such as superconducting states [24, 26, 27, 30, 32, 36, 39, 41, 44, 47, 48, 61, 76, 78, 87, 95, 108, 114], topological states [24, 45, 47, 90, 110, 251] and magneto-electric states [84, 95, 252, 253]. These properties promote altermagnets as intriguing materials for information technology.

Like many other quantum states of matter, the novel physics and potential applications of altermagnetism rely on the distinct electronic structure embedded in the hosting materials. Consequently, it is a major task of altermagnetism study to investigate the spin splitting and polarization of the band structure in candidate materials following the theoretical prediction. Although theoretical studies have advanced rapidly in predicting altermagnetic materials and their intriguing properties, experimental verification and material realization remain in their early stages. In particular, this field is challenged by the limited number of desired materials, and the conflicting results that need to be reconciled for several workhorse candidates under ongoing investigation. Currently there are several comprehensive reviews and concise perspectives on altermagnets research [12, 16, 35, 63, 99, 113, 125, 127, 254, 255], most of which aim at a general and didactic description on the exciting aspects of altermagnetism, yet without addressing the reality that experimentally demonstrated altermagnets are scarce and the workhorse candidates are under strong debate. This might deliver over-optimistic illusions to those from related fields. It is thus one of our responsibilities in this review to explicitly present the status of experimental efforts, besides an understandable description on the concept and progress of altermagnetism. We also give an introductory insight, from a point of view of condensed matter experimentalist, on the key features that can define an altermagnet, by discriminating between T-symmetry breaking spin symmetry and T-symmetry breaking responses. We point out several guidelines for experimental investigation of altermagnetism and desirable characteristics which we prefer in an ideal altermagnet, to possibly guide the material exploration and fulfill the tempting potential of altermagnetism.

2. Defining characteristics of altermagnetism

2.1. What is altermagnetism?

In conventional collinear ferromagnets, only one type of magnetic lattices exists and the ferroic alignment of magnetic moments leads to macroscopic magnetization (figure 1(A)), generating T-symmetry breaking spin polarization in the band structure and constant energy contours (CECs) in reciprocal space (figure 1(D)). In conventional collinear antiferromagnets, opposite magnetic sublattices are linked by combinations of T-symmetry and spatial operations including inversion (P) or translation (τ) symmetries (figure 1(B)), resulting in spin degenerated (T-symmetric) CECs in reciprocal space (figure 1(E)). The term 'altermagnetism' is introduced to describe the alternating spin polarizations presented in both real (figure 1(C)) and reciprocal (figure 1(F)) space, which is characteristic of this new magnetic state of matter [12, 16, 17]. Altermagnets are unconventional compensated magnetism of which the magnetic sublattices are connected by crystal symmetry operations (C) including rotation, mirror, glide and screw, rather than P or τ, giving rise to C-paired spin momentum locking (SML) of the band structure in reciprocal space (figure 1(F)), which is T-symmetry breaking.

On the one hand, the alternating alignment of magnetic moments in real space leads to compensated magnetization globally, *i.e.*, zero net magnetization as antiferromagnets have. Such compensating alignment leads to robustness against external magnetic field perturbation, the absence of parasitic stray fields and ultrafast dynamics. Meanwhile, the breaking of such symmetry, say, by strain or field, together with the T-symmetry breaking SML in altermagnetism, is capable of generating large magnetotransport effects [256], and unconventional piezomagnetism [8, 34, 57, 77, 212], holding great potential in spintronics applications such as terahertz nano-oscillators [257]. On the other hand, the C-paired SML solely arising from the non-relativistic, anisotropic exchange interactions rather than relativistic spin–orbit coupling (SOC) or subtle correlated instabilities in metallic Fermi fluids [99, 258, 259], promises charge–spin conversion effect [3, 7, 97, 128, 203–211] at ambient conditions in a variety of metallic and insulating materials. This mimics ferromagnets which facilitate the readout and writing functionalities in magnetic random-access memories (MRAMs) through TMR, spin-transfer torque or spin–orbit torque effects. Furthermore, altermagnets are allowed to have T-symmetry breaking responses such as the AHE [1, 65, 124, 177, 224–235, 260], the anomalous Nernst effect (ANE) [242–245], MOKE [82, 106, 236, 237] and circular dichroism (CD) [103, 189, 213–223].

Besides these T-symmetry breaking properties, the compatibility of altermagnetism with other novel states of matter including superconductivity, band topology and (anti)ferroelectricity in one material offers valuable chances to explore exotic quantum states of matter and macroscopic quantum phenomena. The connection between altermagnetism and superconductivity is naturally realized by the

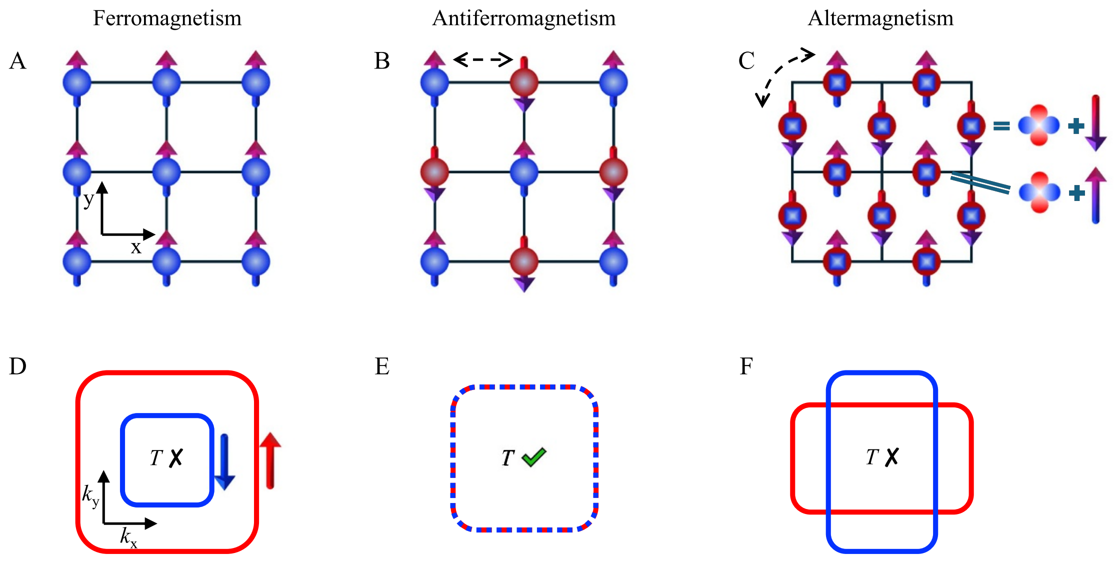

Figure 1. The correspondence between collinear magnetic structure in real space and spin-dependent constant energy contours (CECs) in reciprocal space. Redrawn according to reference [99] (A) Conventional collinear ferromagnetism with a parallel/-ferroic alignment of atomic magnetic dipoles. (B) Conventional collinear antiferromagnetism with anti-parallel alignment of atomic magnetic dipoles. The dashed double-headed arrow indicates the translational or inversion symmetry between the anti-ferromagnetic sublattices. (C) Schematic altermagnetism with decomposition of the local anisotropic spin density into antiferroically aligned dipoles (colored arrows) and ferromagnetically aligned higher-partial-wave (d-wave) spin-density component [99, 255]. The dashed double-headed arrow indicates the rotation, mirror, glide or screw symmetry operations between the altermagnetic sublattices. (D) Ferromagnetic spin polarized CECs for the uncompensated majority- and minority-spin in reciprocal space, showing T-symmetry breaking. (E) Antiferromagnetic spin degenerated CECs preserving T-symmetry. (F) Altermagnetic spin polarized CECs present the corresponding anisotropic (d-wave) order breaking the T-symmetry. Red and blue (solid and dashed) lines or arrows in (D)–(F) indicate the spin polarization direction.

proposal of possible altermagnetism in La_2CuO_4 as a typical parent compound of cuprate high-T_c superconductors [17]. Other cuprates [108] and ruthenates [78] are also altermagnetic candidates [114]. Based on superconductor/altermagnet junctions, novel superconducting phenomena have been discussed, such as orientation dependent Josephson effect, Andreev reflection and superconducting diode effect [26, 27, 30, 36, 41, 44, 61, 87]. The d-wave altermagnetism also enables Majorana modes [24, 47], finite-momentum Cooper pairing and mixed s-wave and p-wave pairings [32, 39, 76]. These potentially offer a new platform for superconducting spintronics [48, 95, 261]. The distinct spin symmetry in real space and reciprocal space, and the inherent spin polarization in the electronic structure of altermagnetism not only give rise to topological Weyl quasiparticles and Fermi arcs [164, 201], but also bulk magnetic topological states and the potential realization of orientation-dependent quantum AHE [45, 58, 90, 110, 251]. Multiferroic materials that combine ferroelectricity and altermagnetism provide the chance to integrate altermagnetic spin polarization and electrical polarization [84, 145, 146], not only enriching the spectrum of magnetoelectric coupling but also paving the way for electrically controlled spintronic and multiferroic devices.

2.2. Characteristic of altermagnetism

With the advance of antiferromagnetic spintronics [256], antiferromagnetic materials possessing diverse magnetic structure symmetry, band spin polarization symmetry, and particularly optical, electrical, thermal responses have gained widespread attention. This leads to the introduction of terminologies such as ‘spin-split antiferromagnets [72]’, ‘non-collinear antiferromagnets [262, 263]’, ‘Anomalous Hall antiferromagnets [15]’, ‘odd/even-parity magnets [264, 265]’, ‘T-symmetry breaking/conserving SML’ and ‘T-symmetry breaking responses’. Since each of these terms focuses on different facet of the studied magnetism, with the latter three rigorously defined by symmetry while the others not, conceptual overlaps are unavoidable, leading to potential misunderstanding. From the standpoint of a condensed matter experimentalist, it is necessary to properly differentiate between the T-symmetry of SML in reciprocal space and T-symmetry breaking responses for different types of altermagnets, yet the recent literatures often fail to do so. For example, it is a common misunderstanding to assume that one type of T-symmetry breaking, such as T-symmetry breaking SML, inherently corresponds to T-symmetry breaking responses, such as AHE/ANE, or vice versa. Another example is to simply use the term

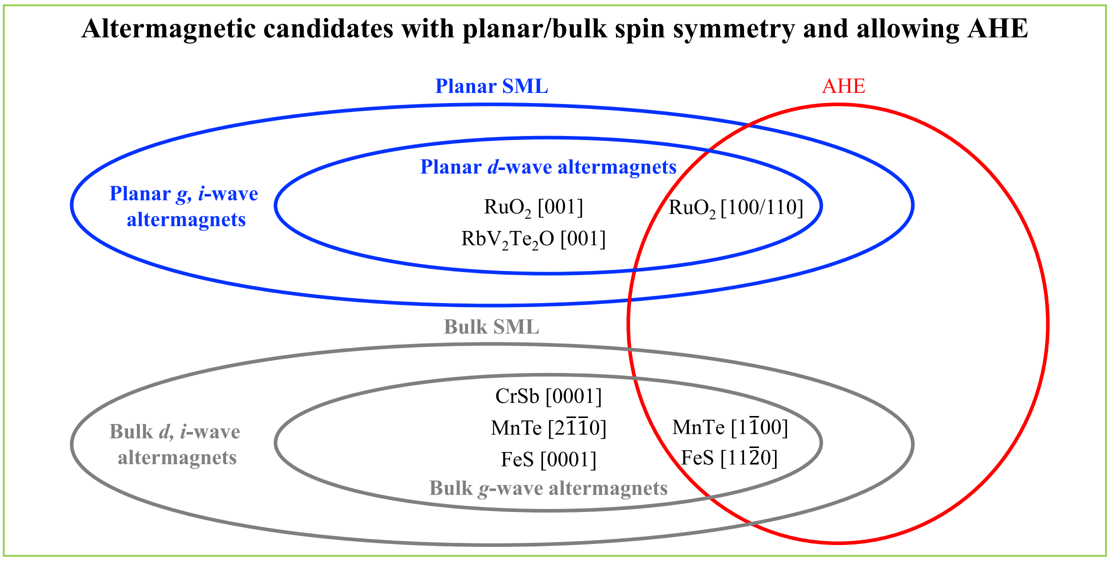

Figure 2. Canonical altermagnetic candidates, described by their planar/bulk spin symmetries in the three-dimensional BZ, depending on whether there is a nodal plane at $k_z = 0$. Those allowing AHE are also specified with the Néel vector orientations.

'T-symmetry breaking' to describe the angle-resolved photoemission spectroscopy (ARPES)-measured spin polarization symmetry in two-dimensional momentum space. As both SOC type SML and bulk altermagnetic SML exhibit antisymmetric spin polarization when reversing only two components of momentum (i.e., $E(k_x,k_y,\uparrow) = E(-k_x,-k_y,\downarrow)$), just observing such asymmetry in one specific two-dimensional momentum plane determined by the photon energy is not enough to establish the T-symmetry breaking SML in altermagnet.

According to the characteristic spin-group integer, defined as the number of nodal surfaces crossing the Γ-point in the whole Brillouin zone (BZ), the spin polarization symmetry in altermagnets can be classified as d-wave (2), g-wave (4), and i-wave (6). Furthermore, depending on the presence or absence of nodal surface at $k_z = 0$, such symmetry can be planar or bulk. The combination of these two classification generates totally 6 types of anisotropic symmetries, which is explicitly shown in the supplementary figure 2 of [17]. Since ARPES measurement using one single photon energy is only able to measure the band structure in a quasi-planar momentum space, the expected spin symmetry in such space varies for bulk and planar type altermagnets. According to the planar/bulk-d/g/i-classification, planar type anisotropy has symmetric SML in $k_x - k_y$ plane ($E(k_x,k_y,\uparrow) = E(-k_x,-k_y,\uparrow)$) or along k_z($E(k_z,\uparrow) = E(-k_z,\uparrow)$). In contrast, bulk type presents antisymmetric SML both in $k_x - k_y$ plane and along k_z. Consequently, observing an antisymmetric SML using ARPES (for most of the cases, in $k_x - k_y$ plane) at one photon energy is not enough to demonstrate the existence of altermagnetism, since traditional SOC induced Rashba type SML also manifests such antisymmetry. Regarding specific materials, as listed in figure 2, RuO_2 and RbV_2Te_2O belong to planar d-wave altermagnets with symmetric SML in two-dimensional momentum planes. Hexagonal α-MnTe, CrSb and FeS, instead, belong to bulk g-wave type with antisymmetric SML in momentum planes. Note that all types of collinear altermagnets have even-parity symmetry. Hexagonal Mn_3Sn has been proved to exhibit T-symmetry breaking responses such as AHE [266, 267], yet its T-symmetry breaking SML remains to be demonstrated in experiment. Odd-parity magnets exhibit T-symmetric, nonrelativistic spin splitting [268–270], for which the characteristic SML awaits direct experimental confirmation.

SOC in an altermagnet (where T-symmetry is broken) can create weak ferromagnetism or weak ferrimagnetism and allows for an AHE that depends on the direction of the Néel ordering vector [79, 123]. In a spin-split, compensated magnet like altermagnet, the absence of SOC means that the symmetry operations of spin and lattice are separated, which can be described by spin groups. AHE, except topological Hall effect, on the other hand, is a relativistic effect, for which the magnetic materials should be described by magnetic groups in which SOC locks the lattice and spin rotations. The distinct symmetry groups describing magnets which allow for AHE and altermagnets which show T-symmetry breaking SML leads to separate pools of materials. For example, d-wave altermagnet RbV_2Te_2O presents planar type spin polarization in momentum space, but no AHE given its Néel vector along [001]. *G*-wave altermagnet α-MnTe exhibits bulk type SML in $k_z \neq 0$ momentum planes (without SOC) for Néel vectors aligned with $[1\bar{1}00]$, [0001] and $[2\bar{1}\bar{1}0]$ directions, but only the first one allows AHE [228].

3. Band structure and spin polarization study of candidate altermagnets

Having defined the key characteristics of altermagnetism, the core mission remains to realize such state of matter in real materials. One natural question arises: what kind of approaches could provide sufficient and necessary evidence to demonstrate the existence of altermagnetism in a material? According to the previous section, the distinction of altermagnetism from conventional antiferromagnetism lies in the *C*-paired sublattice symmetry. Thus, diffraction methods such as powder or single-crystal neutron diffraction can in principle directly detect the altermagnetic order [170, 176]. However, the value of altermagnetism is more about its novel phenomena and responses rather than structure. The characteristic *T*-symmetry breaking SML composes the vital evidence one should provide to demonstrate the altermagnetism.

3.1. Status of altermagnetic material exploration

In recent years, guided by spin group symmetry analysis and supported by density functional theory (DFT) calculations, a growing number of candidate altermagnetic materials have been identified [10, 17, 21, 31, 40, 53, 67, 71, 80, 130]. These include RuO_2 [1, 7, 17, 203–205], RbV_2Te_2O [192], KV_2Se_2O [196, 271], MnTe [183, 184, 186, 188], CrSb [185, 187, 191, 202], FeS [229], $FeSb_2^9$ [272, 273], Mn_5Si_3 [231–233], $CoNb_4Se_8$ [274–277], MnF_2 [37, 58, 278], FeF_2 [279], $CaMnO_3$ [278, 280], MnO_2 [281], ReO_2 [38], $LiFe_2F_6$ [282], RuF_4 [283], κ-Cl [3, 284], and others. Their non-relativistic spin-splitting properties have been investigated using a variety of experimental techniques, ranging from diffraction, microscopy, spectroscopy to transport measurements. ARPES provides direct evidence for the alternating lifting of spin degeneracy in momentum space—*T*-symmetry breaking SML. The most direct experimental confirmation of altermagnetism is achieved by probing its spin-dependent electronic bands via spin-resolved ARPES (SpinARPES). This section first presents, in table 1, a summary of key parameters for experimentally identified candidate altermagnetic materials, covering space group, conductivity, magnetic ordering temperature, band splitting, spin polarization, and other relevant properties. Following this, we focus on a detailed review of experimental results concerning the band structure and spin polarization of several mainstream altermagnetic candidates: RbV_2Te_2O/KV_2Se_2O, RuO_2, α-MnTe, CrSb, and $CoNb_4Se_8$.

3.2. D-wave altermagnet RbV_2Te_2O

The experimental study on *d*-wave altermagnets, RbV_2Te_2O family is inspired by the initial theoretical predictions by Ma *et al* [8] who first identified that a novel type of SVL, termed *C*-paired SVL, in antiferromagnetic systems, can be realized in monolayer V_2Se_2O and V_2Te_2O. As shown in figure 3, in *C*-paired SVL, spin-polarized valleys are connected by crystal symmetry *C* (e.g. rotation or mirror) such that $E_\uparrow(K) = E_\downarrow(CK)$. Distinct from conventional *T*-paired SVL, where spin-split valleys are related by time-reversal symmetry *T* ($E_\uparrow(K) = E_\downarrow(-K)$) and rely on strong SOC and broken inversion, *C*-paired SVL originates from strong exchange coupling between itinerant electrons and the underlying antiferromagnetic order. This mechanism can generate spin splitting up to several EVs in the absence of SOC. Enforced by the crystal's rotational symmetry, this polarization manifests as *C*-paired SVL, where the opposite spin is locked to opposite valleys (*K* and K'). Consequently, the observation of *C*-paired SVL serves as a definitive electronic signature of the altermagnetic state, while the altermagnetism provides the strong intrinsic spin splitting necessary for robust valleytronic functionality.

Following this prediction, the authors' group [192] studied an analogous layered material RbV_2Te_2O (figure 4(A)) using SpinARPES, scanning tunneling microscopy/spectroscopy (STS) and first-principles calculations, demonstrating its uniqueness as a room-temperature ordered ($T_N > 307\ K$), metallic, layered, *d*-wave altermagnet. Figure 4(C) presents the ARPES band spectra measured along high-symmetry paths at 12 K, overlaid with the corresponding calculated dispersion. Structural and magnetic symmetries govern the electronic properties of RbV_2Te_2O, leading to a Fermi surface exhibiting four-fold rotational symmetry and diagonal mirror operations connecting reciprocal-space valleys. Low-energy band structure is dominated by three sharp bands (α, β, γ), with first-principles calculations revealing alternating spin polarization along *X*–*M* vs *Y*–*M* and consistent spin ordering among α, β, γ. The excellent agreement between theory and ARPES measurements conclusively establishes *C*-paired SVL in this layered room-temperature antiferromagnet. Furthermore, the alternating spin polarization has been directly

Table 1. The key properties of the candidate altermagnets experimentally investigated. M: metal; S: semiconductor; SML: spin–momentum locking; AM: altermagnet; NM: nonmagnetism. E_F: Fermi level; AHE: anomalous Hall effect; ANE: anomalous Nernst effect; SSMR: spin-splitting magnetoresistance; μSR: muon spin rotation; GMR/TMR: giant/tunneling magnetoresistance; XMCD: x-ray magnetic circular dichroism; ARPES: angle-resolved photoemission spectroscopy; DFT: density functional theory.

Candidate	Space group	Conduction	Parity	T_N (K)	Band splitting	Spin polarization	Other properties
RbV_2Te_2O KV_2Se_2O	P4/mmm	M	*d*-wave AM	>307 [192] 400 [182]	∼1.6 eV. All bands split at E_F.	T-breaking SML at E_F [192,196].	Possible hidden AM [182].
RuO_2	$P4_2$/mnm	M	*d*-wave AM	>300 [171,172]	∼1.4 eV (DFT) along Γ–M and A–Z [1,190]	T-breaking SML at E_F[189].	AHE [225], SSMR [285], MCD-ARPES [189], spin splitting effects [7, 203–209], GMR/TMR [14,23,43,239,240].
			NM	/	Rashba-like splitting [190]	T-symmetric SML [190]	Ordinary Hall effect [286] $m_{Ru} \sim 10^{-4}\mu B$ [178, 179] Fermi liquid [136]
Strained Mn_5Si_3	$P6_3$/mcm	M	*d*-wave AM	∼260 [242]	∼0.2 eV (DFT) [232]	T-breaking SML (DFT) [234]	AHE [231–234], ANE [242–244].
α-MnTe	$P6_3$/mmc	S	*g*-wave AM	267∼310	>0.3 eV [183,186,188], temperature-dependent band splitting [184,186,188]	T-breaking SML [183] T-symmetric SML [195]	Chiral split magnon [246], AHE [228, 230], XMCD [213], piezomagnetic properties [212]
CrSb	$P6_3$/mmc	M	*g*-wave AM	700∼705	⩾0.8 eV [166,185,187,191,201,202]	T-breaking SML [202]	Chiral spin-split magnons [143,223], Néel vector-dependent anomalous transport [224,235,287], XMCD [220], ANE [245].
$CoNb_4Se_8$	$P6_3$/mmc	M	*g*-wave AM	168 [274]	Temperature-dependent band splitting [276]	T-breaking SML [276]	/

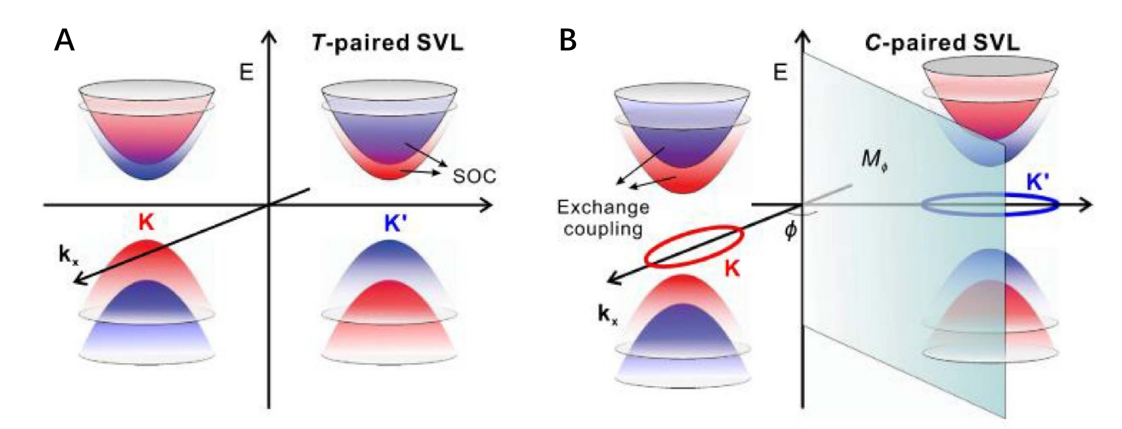

Figure 3. Schematics of T-paired SVL and C-paired SVL. (A) In T-paired SVL, the spin-split bands (spin-up in red, spin-down in blue) arise from strong SOC under broken inversion symmetry, and the two valleys are connected by time-reversal symmetry. (B) In C-paired SVL, the spin splitting originates from exchange coupling between itinerant electrons and local magnetic moments, while different valleys are connected by a crystal symmetry C, such as a mirror symmetry M_ϕ Reproduced from [8]. CC BY 4.0.

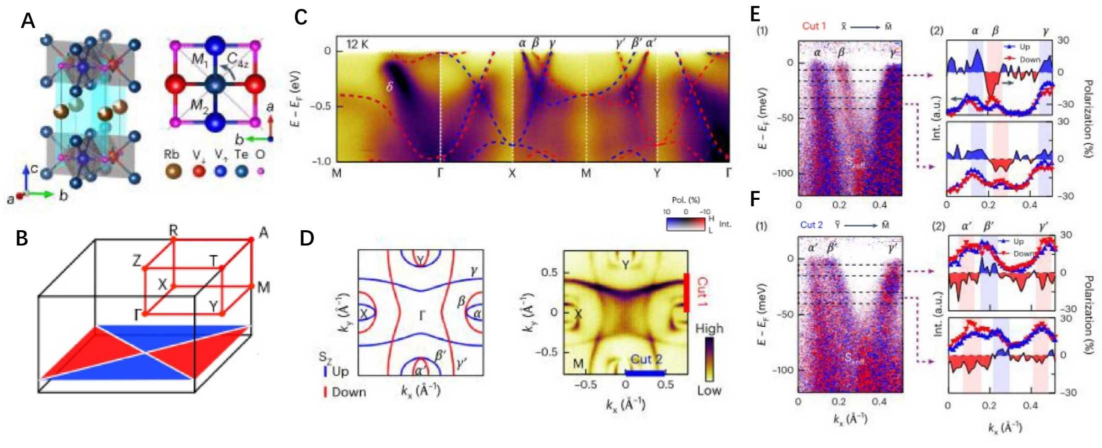

Figure 4. C-paired SVL in d-wave altermagnet RbV_2Te_2O. (A) Crystal structure of RbV_2Te_2O, where the arrows indicate the magnetic moments of V that are parallel/antiparallel to the c-axis. Opposite-spin sublattices are connected by diagonal mirror symmetry M_1 and M_2 (transparent blue planes) and four-fold rotation symmetry (C_{4z}). (B) The bulk Brillouin zone shows a pattern of alternating spin polarization across adjacent valleys, represented by blue and red regions. (C) Band structure of RbV_2Te_2O along high-symmetry paths. The dashed red and blue lines denote first principles calculated bands with opposite spin polarizations. Bands labeled α, β, γ and α', β', γ' are connected by diagonal mirror symmetry and exhibit spin splitting induced by the C-paired AFM order. Band δ arises from surface reconstruction associated with Rb atoms. Here, the ARPES data were collected at $T = 12\ K$. (D) The calculated spin-resolved Fermi surface for the altermagnetic phase and ARPES mapping at $h\nu = 69$ eV. (E, F) Band spin polarization. Spin-resolved band spectra and their corresponding momentum distribution curves (MDCs) along the high-symmetry cuts X–M (cut1) and Y–M (cut2). All SpinARPES spectra are taken with photon energy $h\nu = 21.2$ eV. Int., intensity; Pol., polarization; H, high intensity; L, low intensity. Reproduced from [192], with permission from Springer Nature.

proved via SpinARPES. As shown in figures 4(E) and (F), SpinARPES measurements along mirror-symmetric momentum cuts (cut 1: $\bar{X} - \bar{M}$ and cut 2: $\bar{Y} - \bar{M}$) reveal opposite spin-polarization symmetries along the two directions, directly confirming C-paired SVL in RbV_2Te_2O. Through analysis of the quasi-particle interference pattern in STS mapping (shown in the figure 4 in [192]), it is further revealed a strong suppression of intervalley scattering—a phenomenon originating from the spin selection rules imposed by spin–momentum locking, which directly manifests the SVL mechanism under weak SOC. All these results establish RbV_2Te_2O as a layered room-temperature antiferromagnetic metal featuring alternating magnetic sublattices and a novel type of symmetry-driven spin splitting. It provides an ideal material platform for both fundamental studies and potential device applications in spintronics and valleytronics.

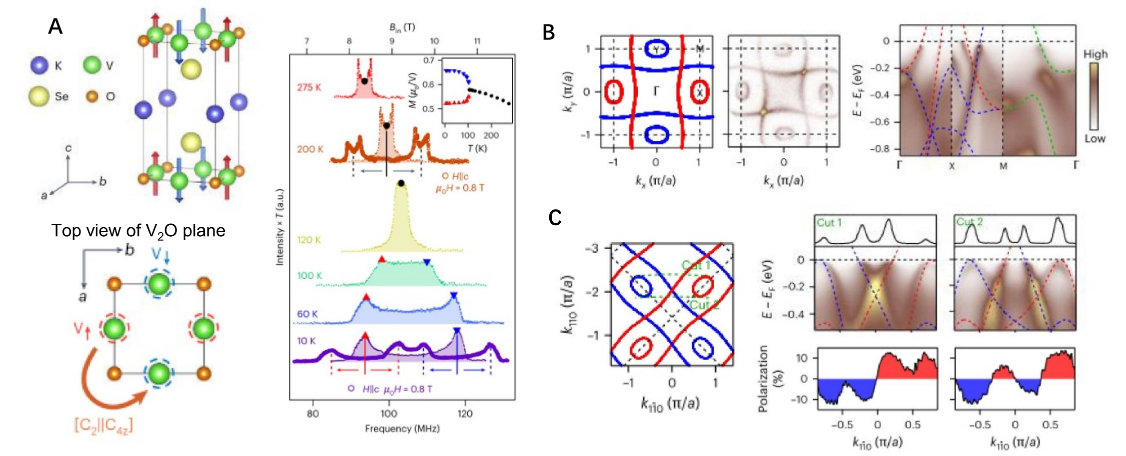

Figure 5. Altermagnetism in KV_2Se_2O. (A) The crystal and magnetic structures of KV_2Se_2O, along with its temperature-dependent ^{51}V frequency-sweep NMR spectra. Red and blue dashed circles around the V atoms indicate up and down spins. The inset plots the magnetic moment M of V atoms as a function of temperature T. (B) Electronic structure of KV_2Se_2O, including calculated spin-resolved Fermi surfaces, ARPES measured Fermi surface and band spectra. Red, blue and green curves represent spin-up, spin-down and spin-degenerate bands. (C) Spin-polarized features of KV_2Se_2O measured via SpinARPES, including band spectra along cuts 1 and 2 through the spin-resolved Fermi surfaces, and momentum-dependent spin polarizations exhibiting an asymmetry between spin-up and spin-down states. Reproduced from [196], with permission from Springer Nature.

Almost simultaneously, Jiang *et al* [196] reported room-temperature altermagnetism with *d*-wave spin–momentum locking in the quasi-two-dimensional metallic oxide KV_2Se_2O. Through magnetic susceptibility, nuclear magnetic resonance (NMR), and neutron diffraction measurements, they have unambiguously confirmed the presence of a magnetic ordered state in KV_2Se_2O, with the magnetic moments aligned along the crystallographic *c*-axis, shown in figure 5(A). Furthermore, they also investigated its band structure using photon-energy-dependent ARPES, revealing a simple quasi-two-dimensional electronic structure that aligns well with first-principles calculations, shown in figure 5(B). Compared with band calculation, they found that the bands along the high-symmetry direction $\Gamma - X - M$ are spin splitted, whereas the bands along $\Gamma - M$ remain spin degenerate, in consistent with the *d*-wave symmetry. The momentum-dependent spin-splitting, which originates from anisotropic crystal fields, reaches 1.6 eV at E_F, one of the largest values reported among altermagnets. Figure 5(C) shows the spin polarization of the band spectra measured via SpinARPES. Two momentum cuts crossing the Fermi surface reveal a characteristic spin-polarization sequence. Along cut 1, the spin polarization of the corresponding bands exhibit a down–down–up–up ordering, while for cut 2, it is a down–up–down–up spin sequence. These spin textures confirm the unconventional *d*-wave altermagnetism in KV_2Se_2O.

Notably, while SpinARPES measurements have unambiguously demonstrated that RbV_2Te_2O and KV_2Se_2O exhibit room-temperature *d*-wave altermagnetism, characterized by a *T*-symmetry breaking SML, recent neutron diffraction experiments yielded the opposite conclusion. Through neutron diffraction studies of polycrystalline and single-crystal samples, Sun *et al* [182] revealed a G-type antiferromagnetic order in bulk KV_2Se_2O at room temperature. This finding contradicts the C-type magnetic structure previously considered essential for *d*-wave altermagnetism, indicating that bulk KV_2Se_2O is not an intrinsic altermagnet. The apparent discrepancy likely arises from the surface-sensitive nature of photoemission measurement, which probes primarily the topmost V_2Se_2O layer of the cleaved crystal KV_2Se_2O, whereas neutron diffraction averages over the bulk KV_2Se_2O magnetic order. This aligns with theoretical predictions that altermagnetic properties originate from the monolayer V_2Se_2O limit and suggests the existence of hidden altermagnetism in KV_2Se_2O. Consequently, the application of bulk KV_2Se_2O in altermagnetic spintronics may face limitations, underscoring the need for further exploration of genuinely two-dimensional altermagnetic materials.

3.3. RuO_2

RuO_2 adopts the rutile structure with space group $P4_2/mnm$, as shown in figure 6(A). In this structure, each Ru atom is coordinated by six O atoms, forming a slightly distorted octahedron [288]. Notably, neighboring oxygen octahedra are connected through rotation rather than translation. The specific connectivity, combined with antiferromagnetic alignment of spins at the Ru sites, is predicted to give rise to a characteristic *d*-wave altermagnetic ground state with zero net magnetization that simultaneously exhibits ferromagnetism-like lifted Kramers spin degeneracy (LKSD) in reciprocal space (figure 6(A)).

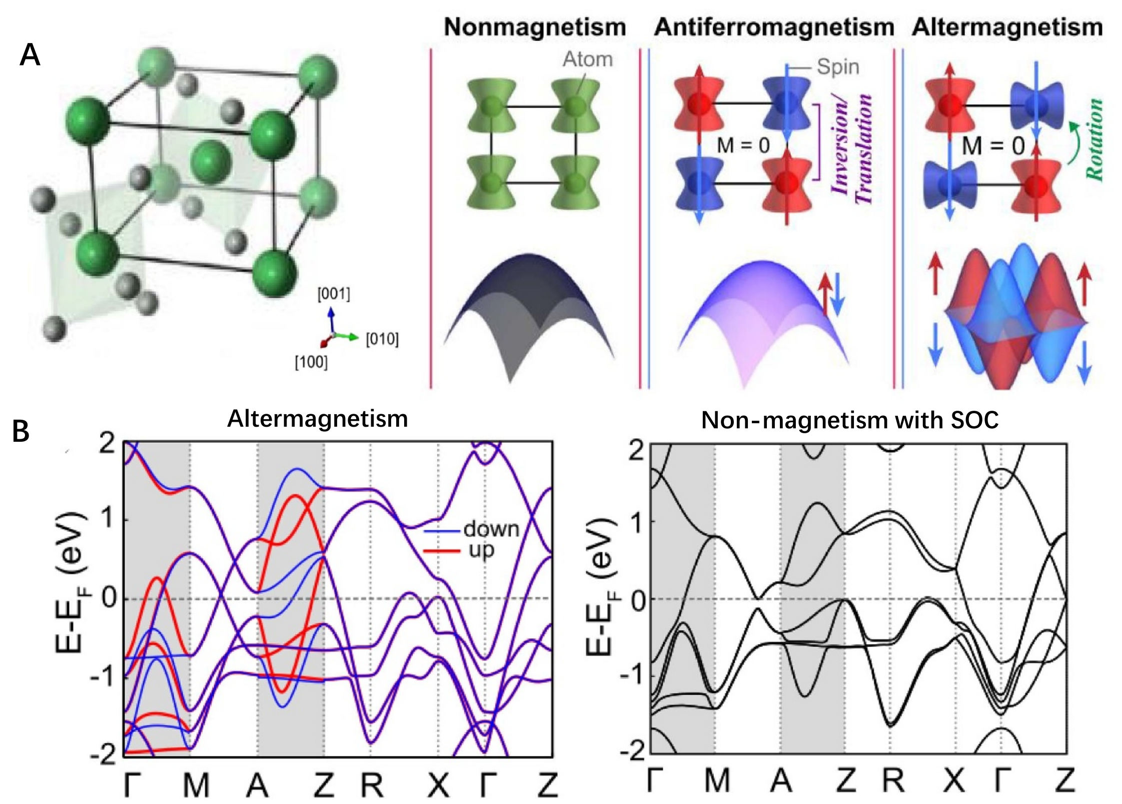

Figure 6. The crystal and band structure of RuO_2. (A) The crystal structure of RuO_2 in real space and the categorization of the magnetism of RuO_2: nonmagnetism, antiferromagnetism, and altermagnetism. (B) Electronic structure calculations along high-symmetry lines for the altermagnetic phase with a static $U = 1.3$ eV correction on the Ru site and nonmagnetic phase of RuO_2 with SOC, respectively. Reprinted (figure) with permission from [190], Copyright (2024) by the American Physical Society.

Furthermore, first-principles calculations confirm that an altermagnetic state in RuO_2 induces spin-splitting along the $\Gamma - M$ and $A - Z$ directions, whereas a nonmagnetic configuration retains full band degeneracy, as shown in figure 6(B). RuO_2 is predicted to possess a significant spin splitting of up to 1.4 eV, along with the presumed magnetic ordering well above room temperature [1]. Due to its substantial spin splitting and a high critical temperature, RuO_2 is considered a highly promising material for modern spintronics. These attributes could enable faster and more energy-efficient spin-based information processing in devices, heralding significant potential for future applications.

The prediction of altermagnetism in RuO_2 is corroborated by numerous spin transport results. Feng *et al* [225] reported an AHE in RuO_2 films with a conductivity exceeding 1000 $\Omega^{-1}\mathrm{cm}^{-1}$, which is over both the ordinary Hall contribution and that arising from a weak field-induced magnetization, attributed to the compensated collinear magnetic order. Tschirner *et al* [227] revealed a saturation of the AHE under high applied magnetic fields, which is consistent with the expected Néel-vector reorientation field. Bose *et al* [204] revealed that RuO_2 produces a spin current with a tilted spin polarization aligned approximately with its Néel vector by angular-resolved measurements of the full torque vector. These results have been interpreted as hallmarks of the altermagnetic order. More recent studies have further solidified this perspective by extensively probing the altermagnetic spin splitting effect with a variety of methods, such as spin Seebeck effect, electrical transport, spin splitting torque, and terahertz (THz) emission measurements [14, 203, 205–211, 240]. It was experimentally observed that RuO_2 exhibits crystallographic-axis dependent spin-to-charge conversion efficiency, reversible and inverse spin-splitting effect, spin-splitting magnetoresistance, electrical manipulation of spin splitting torque, and anisotropic THz emission.

However, the magnetic nature of RuO_2 remains a subject of intense debate. Early investigations, employing techniques such as polarized neutron diffraction [171] and resonant x-ray scattering [172], reported evidence consistent with antiferromagnetic ordering in both bulk and thin film samples, forming an initial consensus. Yet more recent and highly sensitive local-probe studies have fundamentally challenged this view. Muon spin rotation/relaxation (μSR) experiments, which are exceptionally sensitive to weak internal magnetic fields, detected either an extremely small ordered moment (on the order of [10–4] μ_B/Ru) or a complete absence of long-range magnetic order in high-quality RuO_2 crystals and

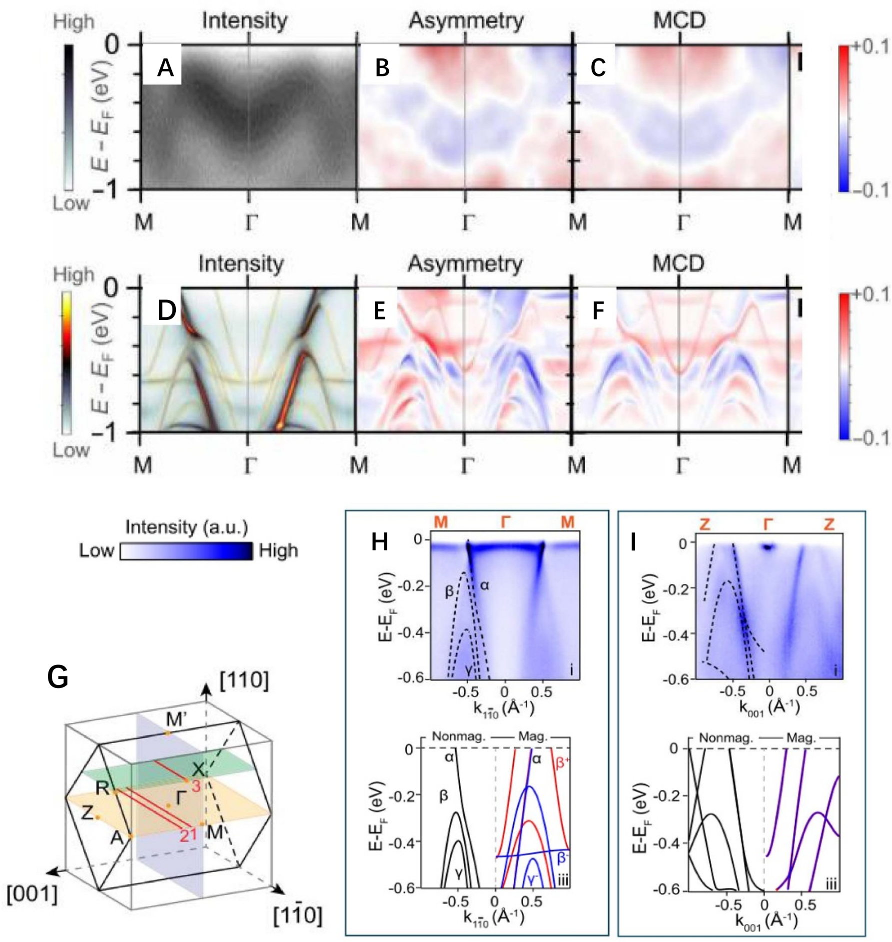

Figure 7. Comparison of experimental MCD and band dispersion of RuO_2 with theoretical calculations. (A) Bands along the $M-\Gamma-M$ measured at 70 K. (B) Measured intensity asymmetry, $A(E_B,0,k_y)$. (C) MCD A_{MCD} $(E_B,0,k_y)$ extracted from the asymmetry. (D) Calculated spectral density average and (E) its asymmetry for circular right and left polarization of the incident light within the experimental geometry. (F) The theoretical MCD extracted. (G) 3D BZ of RuO_2, with yellow and green planes showing high symmetry planes $\Gamma-M-A-Z$ and $R-X$. (H) and (I) The band dispersion of RuO_2 along $\Gamma-M$ and $\Gamma-Z$, compared with nonmagnetic/altermagnetic calculations, respectively. Red and blue lines represent band spin polarization. (A)–(F) Reproduced from [189]. CC BY 4.0. (G)–(I) Reprinted (figure) with permission from [190], Copyright (2024) by the American Physical Society.

films [178, 179]. These results are corroborated by bulk-sensitive spectroscopic techniques like broadband infrared spectroscopy [136]. The stark discrepancy has led to a re-examination of the earlier data, with suggestions that the observed signals in some neutron diffraction studies may be attributed to artifacts rather than true magnetic order. Consequently, the previously assumed altermagnetic ground state in RuO_2, predicated on robust AFM order, is now under significant debate, highlighting the critical importance of sample quality and the choice of bulk-sensitive local probes in determining its true magnetic state.

The unique spin groups delineating altermagnetic order in both position and momentum spaces result into non-relativistic spin splitting of the bands. ARPES serves as a key experimental tool for probing such spin splitting, enabling direct characterization of the momentum-resolved spin polarization. Recently, various ARPES-based techniques have been used to study the electronic structure of RuO_2. By finding magnetic circular dichroism (MCD) in the angular distribution for both soft x-ray and ultraviolet photon excitation, Fedchenko *et al* directly confirmed a pronounced time-reversal symmetry-breaking signatures in the electronic band structure of RuO_2 films [189], shown in figures 7(A)–(F). Since dichroism in ARPES is per se a matrix element effect, which depends on the initial and final states as well as on the perturbation by the light field, the lack of systematic orientation dependent and photon energy dependent CD measurements calls for reexamination of the reported magnetic behavior. Subsequently, Liu *et al* [190] conducted comprehensive ARPES and SpinARPES investigations on both thin-film and single-crystal rutile RuO_2. Their study systematically examined the Fermi surface topology and band dispersions along high-symmetry directions, in combination with DFT calculations. Their results reveal that the expected band splitting characteristic of an altermagnetic state is not observed. As shown in figures 7(H) and (I), their experimental measurements along the $\Gamma - M$ direction reveal only three bulk bands near E_F: an electron-like α band crossing E_F, and two hole-like bands (β and γ) with their band tops located approximately 0.2 eV and 0.4 eV below E_F, respectively. Only one band crossing E_F was observed within the momentum range of 0–0.5 Å^{-1} along $\Gamma - Z$ direction. This conflicts with the altermagnetic prediction. According to the proposed altermagnetic state in RuO_2, all low-lying bulk bands are expected to exhibit lifted spin degeneracy except those along the $\Gamma - Z$ direction, which are connected by the screw rotation operation $S_{4z} = \{C_{4z} \mid (1/2, 1/2, 1/2)\}$. Along the $\Gamma - Z$ direction, the screw rotation symmetry protects spin degeneracy even in the altermagnetic scenario. Contrary to the predicted two bands crossing E_F, the experimental data reveal only one. The experimental findings support the nonmagnetic scenario in RuO_2, as opposed to the proposed altermagnetic state. Recently, Lin *et al* [198] reported weak sign of splitting between bands β and γ in parallel to $\Gamma - M$ direction using high-resolution soft x-ray spectra measurements. Further theoretical calculations reveal that both the magnetic-order-included and nonmagnetic band structures show approximate agreement with experimental data, indicating that the electronic structure of RuO_2 is considerably complex and difficult to conclusively determine by any single characterization method.

SpinARPES serves as a direct and crucial technique for probing the momentum-dependent band splitting and spin polarization induced by altermagnetism. Liu *et al* [190] also examined the spin polarization of RuO_2 by SpinARPES experiments using a helium lamp with photon energy of 21.2 eV, shown in figures 7(H) and (I). These experimental results demonstrate that the bulk band exhibits significant in-plane spin polarization, with the polarization vector S_{001} displaying an antisymmetric profile relative to the $\Gamma - Z - M'$ high-symmetry plane. This observation stands in sharp contradiction to the prevailing theoretical prediction for an altermagnetic state, wherein the α band is expected to be fully spin-polarized yet symmetric across the same high-symmetry plane. Based on combined theoretical analysis, the authors attribute the observed spin-polarization structure in RuO_2 to a Rashba-like spin splitting induced by broken space-inversion symmetry, rather than to an exchange magnetic mechanism arising from broken time-reversal symmetry.

The above conflicting results, with only canonical works selected, on RuO_2 concerning its very magnetic ground state pose a major challenge in the field as this material facilitates the introduction of altermagnetism concept. With accumulating reports appearing, it is realized that the magnetic ground state of RuO_2 should be very sensitive to the sample quality, epitaxial strain, stoichiometry deviations, extrinsic disorder, interfacial effects and so on, due to its proximity to a quantum phase transition [66, 119]. Those promising transport properties and especially the spin torque reported could be ascribed to the anisotropic spin Hall effect. We shall not go into details concerning these results as the present review focuses on the band structure and spin polarization aspects. We encourage the readers to refer to specialized reviews for more information [109, 289, 290].

3.4. G-wave altermagnet α-MnTe

Before 2022, α-MnTe had long been considered as a conventional collinear antiferromagnet [170, 291–293]. This perception stemmed from focusing solely on the lattice of magnetic Mn atoms while overlooking the crucial role of non-magnetic Te atoms in the magnetism of α-MnTe crystals. α-MnTe has a hexagonal NiAs-type structure with the space group $P6_3/mmc$, where two Mn magnetic sublattices are connected by a six-fold screw axis along the *c*-axis. Below the Néel temperature ($T_N = 307\ K$ for bulk), obtained from temperature-dependent susceptibility measurements under various magnetic field directions [184] in figure 8(C), it exhibits an A-type AFM ground state where Mn atoms are ferromagnetically ordered along the in-plane $[1\bar{1}00]$ axis while stacked antiferromagnetically along the out-of-plane *c* direction. The Mn spin sublattices are connected by a non-symmorphic six-fold screw-axis rotation $C_{6z}t_{1/2}$ combined with C_{2y} spin rotation (figure 8(A)). The resulting non-relativistic spin-group symmetry reveals a strong time-reversal symmetry breaking and alternating spin splitting in the band structure outside the nodal planes. Consequently, α-MnTe falls into the *g*-wave altermagnetism category. There are four specific planes where spin degeneracy is preserved: one at the $k_z = 0$ plane and three along the Γ–K directions without SOC, as shown by the gray and blue planes in figure 8(B)[17]. By inclusion of SOC, the spin degeneracy within these nodal planes is lifted, known as weak LKSD [183]. On non-high-symmetry planes, the Kramers spin degeneracy is lifted regardless of the presence or absence of SOC, resulting in alternating spin-splitting signals in the energy band structures, known as strong LKSD [183].

The altermagnetic nature of α-MnTe is supported by both theoretical predictions and experimental observations. In 2022, Šmejkal *et al* [16, 17] theoretically predicted that α-MnTe is a high-parity *g*-wave room-temperature altermagnet with exceptionally large spin-splitting energy bands (1.1 eV).

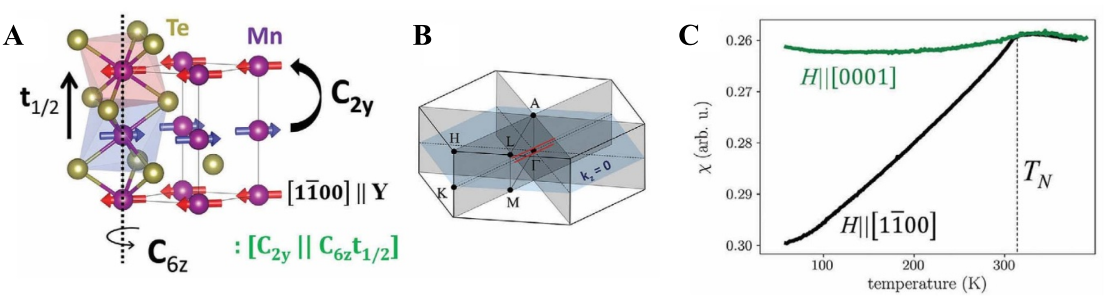

Figure 8. Crystal structure and magnetic properties of α-MnTe. (A) Magnetic structure of α-MnTe with opposing spin sublattices connected by the combined operation of a non-symmorphic six-fold screw-axis rotation $C_{6z}t_{1/2}$ and a C_{2y} spin rotation. The Néel vector is oriented along the $(1\bar{1}00)$ direction. (B) Bulk BZ, displaying the four degenerate nodal surfaces (gray and blue planes). (C) Temperature-dependent magnetic susceptibility χ measured along the (0001) and $(1\bar{1}00)$ axes. Reproduced from [184].

Subsequently, Osumi *et al* [188], Lee *et al* [186], Krempaský *et al* [183], and Hajlaoui *et al* [184] experimentally measured the electronic band splitting of α-MnTe using ARPES, providing spectroscopic evidence for the existence of altermagnetism in α-MnTe.

Specifically, Krempaský *et al* [183] demonstrated that strong LKSD originating from crystalline symmetry exhibits alternating spin splitting, whereas weak LKSD arising from SOC gives rise to non-alternating spin splitting. Meanwhile, the strong altermagnetic LKSD can be identified in the electronic structure only outside the four nodal planes, and the weak altermagnetic LKSD exists within the band structure of the four nodal planes. They compare the measured and simulated ARPES data inside and outside the nodal planes in figures 9(A) and (B). At $k_z = 0.35\text{Å}^{-1}$ ($h\nu = 368$ eV), the path $\bar{\Gamma} - \bar{\text{K}}$ is within one of the nodal planes (figure 9(A)), while $\bar{\Gamma} - \bar{\text{M}}$ path is outside the nodal planes (figure 9(B)). Both experimental and theoretical results reveal a significantly larger band splitting in figure 9(B) (strong altermagnetic), reaching ~ 0.5 eV, in the B_1/B_2 spectral region, compared to the weak altermagnetic case (figure 9(A)). Further, through SpinARPES measurements, they observed the alternating sign of the spin-polarization component along the $\bar{\Gamma} - \bar{\text{M}}$ with the presence of the strong altermagnetic LKSD at a photon energy of 24 eV ($k_z = 0.12\text{Å}^{-1}$) in figure 9(C). However, we noted in another article [184] that a photon energy of 24 eV corresponds to $k_z = 0$, as shown in figure 9(D), implying that the bands are located within the nodal planes. Unexpectedly, different groups have determined the inner potentials of α-MnTe to be 10 eV [194], 11 eV [184] and 16.5 eV [186], respectively, through fitting its photon energy dependent photoemission spectral intensity. In principle, the inner potential fitted for a given material is expected to be consistent across different measurements.

Recently, Zeng *et al* [195] observed *k*-independent Rashba-like spin texture in α-MnTe, which is different from the alternating spin-polarization signals characteristic of altermagnets. Subsequent experiments revealed that this k_z-independent spin polarization stems from emergent surface bands dominated by a Rashba-type spin texture induced by SOC. As shown in figure 9(F), four sharp, hole-like bands emerge at binding energies of 0–0.5 eV. Spin–momentum distribution curve (MDC) measurements along the O_1–B_1 direction (denoted as Cut 1 at $h\nu = 108$ eV, $k_z = 11.5\,\pi/c$) reveal a clear spin polarization signal in these bands, exhibiting a distinct '+−+−' alternating pattern. Shifting the measurement direction from O_1–B_1 (Cut 1) to O_1–B_2 (Cut 2), the spin patterns remain identical. In sharp contrast to the in-plane spin texture predicted for an altermagnet, this behavior aligns perfectly with the Rashba-like pattern expected from an SOC-driven model. Next, they change the incident photon energy to examine whether the spin pattern is k_z-dependent, as predicted in the altermagnet model of α-MnTe. Measurements were performed along Cut 3 ($\Gamma - M$, $h = 120$ eV, $k_z = 12\,\pi/c$) and Cut 4 (O_2–B_3, $h = 129$ eV, $k_z = 12.5\,\pi/c$). As shown in figure 9(F), the spin pattern of the near-E_F bands remains essentially unchanged across the two sides of k_z's within the bulk BZ, persistently showing the '+−+−' configuration. The $k_{||}$- and k_z-independent Rashba-like spin texture suggest its origin from SOC, rather than altermagnetism. Therefore, the lack of comprehensive three-dimensional spin polarization data precludes direct evidence for the proposed altermagnetic order, namely its *g*-wave spin texture. This limitation stems from an insufficient density of momentum points sampled in spin-resolved measurements throughout the bulk BZ. Meanwhile, Zhou *et al* [294] also observed surface states crossing the Fermi level in 50-unit-cell (UC) thick α-MnTe films. The experimentally observed surface states are in agreement with first-principles calculations for α-MnTe with a top Te termination. Furthermore, they

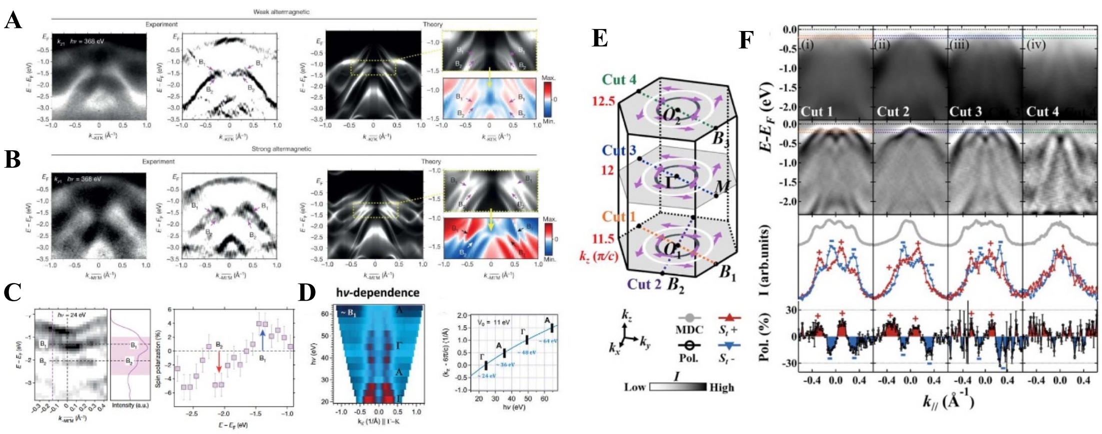

Figure 9. Band structure study of α-MnTe. (A, B) Band spectra showing (A) weak and (B) strong LKSD at $k_z \neq 0$. Measurements were performed using a photon energy of 368 eV and $k_z = 0.35$ Å^{-1} along the (A) $\bar{\Gamma} - \bar{\mathrm{K}}$ and (B) $\bar{\Gamma} - \bar{\mathrm{M}}$ high-symmetry directions. Corresponding one-step ARPES simulations are shown alongside. Red and blue colors indicate opposite spin polarizations. (C) SpinARPES measurements along the $\bar{\Gamma} - \bar{\mathrm{M}}$ direction. Reproduced from [183]. CC BY 4.0. (D) Photon-energy dependent ARPES spectra, assuming a parabolic final-state band and an inner potential of $V_0 = 11$ eV Reproduced from [184]. CC BY 4.0. (E) Bulk BZ of α-MnTe, with two-dimensional cross-sections highlighting the $\bar{\Gamma} - \bar{\mathrm{M}} - \bar{\mathrm{K}}$ planes at three different k_z values. (F) ARPES and SpinARPES data acquired along Cuts 1–4. Cuts 1, 2, 3, and 4 were measured at $k_z = 11.5,\ 11.5\ 12,\ 12.5\ \pi/c$ along the O_1–B_1, O_1–B_2, Γ–M, and O_2–B_3 paths, respectively. Reproduced from [195]. CC BY 4.0.

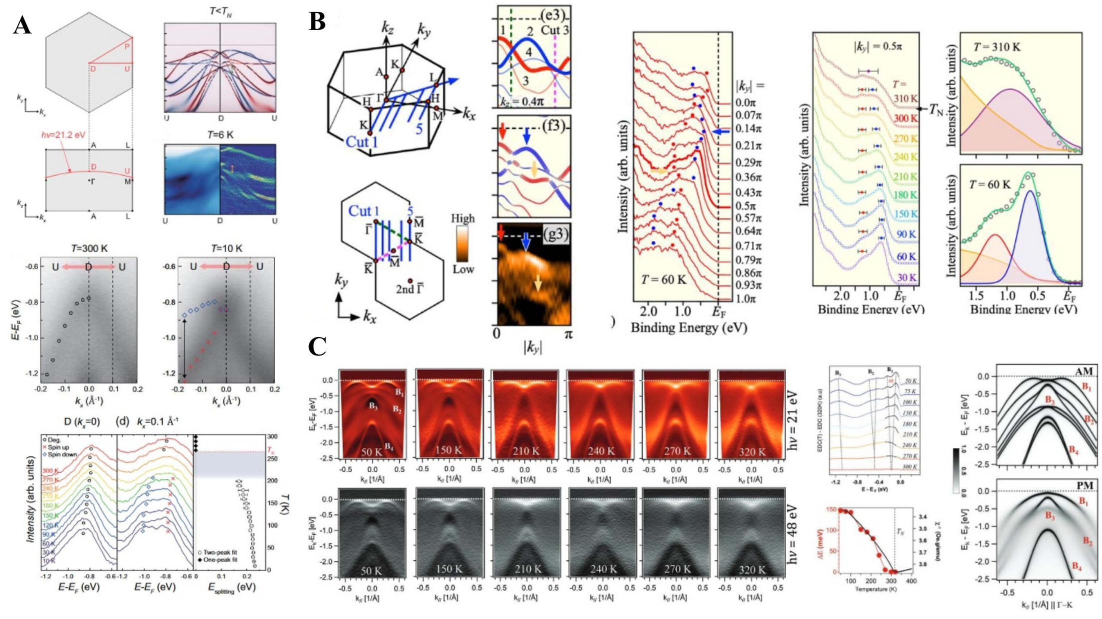

Figure 10. Temperature-dependent band structure of α-MnTe. (A) Calculated bands and ARPES spectra for the paramagnetic and altermagnetic states. Reprinted (figure) with permission from [186], Copyright (2024) by the American Physical Society. (B) Calculated band structures, ARPES spectra and temperature dependence of energy distribution curves (EDCs). Reprinted (figure) with permission from [188], Copyright (2024) by the American Physical Society. (C) Temperature-dependent spin splitting. Reproduced from [184]. CC BY 4.0.

detected a robust AHE and demonstrated that the Hall response arises from the Berry curvature of surface states rather than from bulk bands.

We also note that the large band splitting ($\Delta E > 0.3$ eV) outside the nodal planes measured via ARPES by Lee *et al* [186] and Osumi *et al* [188] correlates with the altermagnetic transition temperature (figures 10(A) and (B)). However, Hajlaoui *et al* [184] found that the SOC-induced band splitting within the nodal planes is also correlated with the magnetic transition temperature in figure 10(C). Therefore, relying solely on the observation of band splitting correlated with the magnetic transition temperature is not entirely sufficient to conclusively verify the altermagnetism.

Given the in-plane magnetic easy axes in α-MnTe, the magnetic structures will form domains with Néel vectors oriented along one of the six equivalent in-plane easy axes. Although the size of these magnetic domains varies with temperature and growth conditions, it is generally much smaller than the typical ARPES beam spot size. Consequently, the band structure is averaged over multiple domains. In ideal models, spin splitting directly translates into complete spin polarization. In contrast, a much lower spin polarization is commonly observed in experiments on real α-MnTe samples. For example, the presence of magnetic domains, often connected by symmetry, tends to average the spin signals of independent domains. This averaging significantly reduces the level of spin polarization in the spin split bands. Therefore, it is often challenging to measure spin polarization of T-symmetry breaking states if multiple domains contribute to opposite signs of spin polarization, by SpinARPES.

In addition, Autieri and Fakhredine [148] extended the study of SML in the altermagnet α-MnTe from the nonrelativistic limit to the relativistic limit. They found that SOC induces antisymmetric exchange interactions and spin canting, leading to the formation of relativistic SML for all three spin components (S_x, S_y, and S_z). In α-MnTe, the dominant S_y component is reduced from g-wave to d_{yz}-wave symmetry due to the breaking of C_{6z} symmetry by the Néel vector along the y axis. The overall relativistic SML comprises S_x (d_{xz}-wave), S_y (d_{yz}-wave), and S_z (s-wave) components. Although the amplitude of the canted spin components in real space is three orders of magnitude smaller than that of the dominant component, their spectral weight in k-space is comparable, significantly influencing k-space-related physical properties such as spin Hall conductivity and spin photocurrents. Moreover, Ye *et al* [295] explored the intrinsic spin and orbital magnetization of the magnetic ground state in the prototypical α-MnTe. They also find that SOC induces weak ferromagnetism through spin canting, along with a slight in-plane rotation of the Néel vector. Remarkably, they identify a net orbital magnetization of 0.176 μ_B per UC oriented along the z-axis, which is two orders of magnitude larger than the spin magnetization (0.002 μ_B) in the same direction. These findings highlight the dominant role of orbital magnetization and its significance for orbital-mediated effects in altermagnets.

3.5. G-wave altermagnet CrSb

As another prototypical g-wave altermagnet, CrSb exhibits a large band splitting ($\Delta E \geqslant 0.8$ eV) along non-high-symmetry directions. This key feature has been directly observed by multiple groups, including those of Yang *et al* [202], Ding *et al* [191], Zeng *et al* [187], Reimers *et al* [185], and Liao *et al* [200], and is consistent with DFT calculations. For example, Zeng *et al* [187] measured the bands along a low-symmetry direction (E–D, Cut 1) and a high-symmetry path (Γ–A, Cut 2). A splitting of $\sim$0.8 eV was observed along E–D (green dashed line in figure 11(A)), while no splitting was resolved along $\Gamma - A$, in agreement with theoretical predictions. Ding *et al* [191] observed spin-split bands on the $(10\bar{1}0)$ cleaved surface. Their photoemission data along D–P–D, alongside calculated spin-split bulk bands, are presented in figure 11(B). By analyzing second-derivative spectra and energy distribution curves (EDCs), they determined a maximum splitting $\Delta \approx 0.93$ eV at $k_z = 0.25$Å^{-1}. Meanwhile, the k_z dependence of this bulk altermagnetic splitting was investigated by Yang *et al* [202]. ARPES spectra along $\bar{\Gamma} - \bar{\mathrm{M}}$ taken at three photon energies (80, 68, and 90 eV) are shown in figure 11(C) (with second derivatives in figure 11(D)). For 80 eV photons ($k_z = 0.28\ c^*$), corresponding to a point outside the nodal planes, two hole-type bands near E_F are observed with a splitting up to 1.0 eV. In contrast, within the nodal planes (68 and 90 eV, $k_z = 0$ and $0.5\ c^*$, respectively), only a single hole band is detected near E_F. This experimentally observed k_z-dependent splitting aligns well with *ab initio* results (green arrows in figure 11(E)). The calculations further show that the split bands at $k_z = 0.28\ c^*$ exhibit strong spin polarization (red/blue curves), whereas the out-of-plane spin polarization $\langle S_z \rangle$ vanishes at $k_z = 0$ and $0.5\ c^*$ (black curves), protected by the $(C_2^S||M_z)$ symmetry. This confirms that the splitting is primarily driven by altermagnetic order, with SOC playing a minor role. Finally, the measured and DFT-calculated $k_x - k_z$ maps (and their second derivatives) in figure 11(F) show remarkable agreement: the altermagnetic splitting is negligible at $k_z = 0$, increases to a maximum near $k_z = 0.25\ c^*$, and decreases back to zero at $k_z = 0.5\ c^*$, conclusively demonstrating the bulk-type altermagnetic character of the splitting in CrSb.

Furthermore, to directly probe the spin polarization of the altermagnetically split bands, SpinARPES measurements were conducted along the $\bar{\Gamma} - \bar{M}$ direction at a photon energy of 80 eV ($k_z = 0.28\ c^*$), where the splitting is near its maximum. Figure 11(G) shows the spin-resolved MDCs extracted along the cut marked by the white dashed line. Both the spin-up and spin-down MDCs display a broadened double-peak structure, corresponding to the spin-split bands. The clear shift in peak positions between the spin-up and spin-down bands directly manifests the momentum-dependent spin splitting characteristic of altermagnetism in CrSb. The spin polarization is extracted and shown. The direct observation of significant spin polarization in the split bands, combined with its excellent agreement with DFT calculations, provides compelling evidence for the altermagnetic nature of the spin splittings in CrSb.

However, from the analysis of the altermagnetic bands in α-MnTe as validated in the previous section, it is known that merely observing a large band splitting and spin polarization at a given k_z

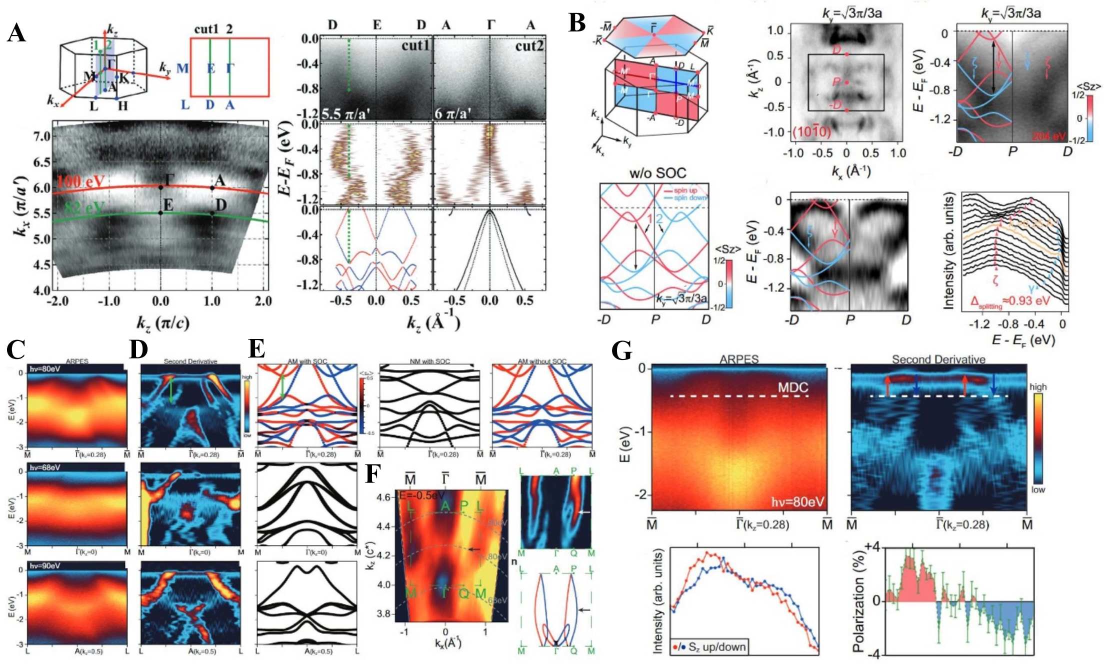

Figure 11. Altermagnetic band splitting and spin polarization in CrSb. (A) Left, photon energy dependent ARPES mapping within the ΓMLA plane. Right, from top to bottom: ARPES spectra, its second-derivative analysis, and DFT-calculated bulk bands along cuts 1 and 2 (measured at photon energies of 82 eV and 100 eV, respectively). Green dashed lines indicate the maximum observed energy separation (∼0.8 eV) of the split bands. Reproduced from [187]. CC BY 4.0. (B) Comparison between the calculated spin-splitting distribution across the ΓMAL plane (and along D–P–D) and the experimentally measured band splitting along D–P–D. The yellow curve is the EDCs at $k_z = 0.25^{-1}$, showing the $\Delta_{splitting} = 0.93$ eV Reprinted (figure) with permission from [191], Copyright (2024) by the American Physical Society. (C) The k_z dependence of altermagnetic splitting along the in-plane $\bar{\Gamma} - \bar{M}$ direction. ARPES spectra taken with 80 eV, 68 eV, 90 eV photons, respectively. (D) The second derivatives of the ARPES spectra corresponding to (C). (E) Spin resolved band structure from DFT calculations. (F) The measured and calculated $k_x - k_z$ map, indicating the spin polarization. (G) Evidence of spin polarization from SpinARPES measurements. Reproduced from [202]. CC BY 4.0.

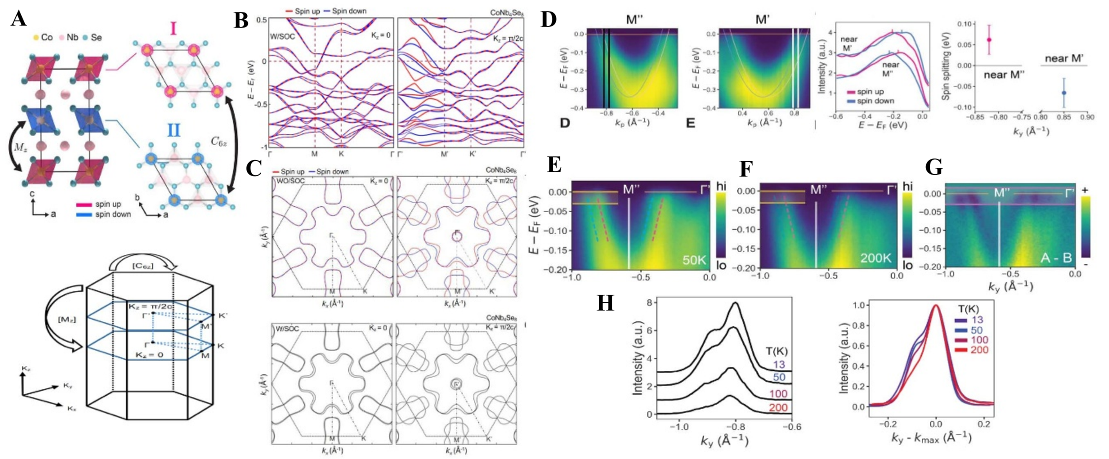

Figure 12. Electronic structure of the altermagnetic candidate $CoNb_4Se_8$. (A) Magnetic structure and the bulk BZ [276, 277]. Reproduced from [276]. CC BY 4.0. (B) DFT-calculated spin-resolved band structures for the nodal plane ($k_z = 0$, along Γ–M–K–Γ) and an off-nodal plane ($k_z = /2c$, along Γ'–M'–K'–Γ'). Red and blue lines denote spin-up and spin-down channels, respectively. (C) Calculated Fermi surfaces at the nodal plane ($k_z = 0$) and an off-nodal plane ($k_z = /2c$), with and without SOC [277],respectively. Reproduced with permission from [277]. (D) Comparison between ARPES measurements and the calculated band structure along $M'' - \Gamma' - M'$. Spin-resolved EDCs at selected momenta (black/white vertical lines) are shown alongside the momentum-dependent spin splitting extracted from the spin-up and spin-down band positions. (E)–(G) Low-energy ARPES spectra along $M'' - \Gamma' - M'$ at $T = 50$ K and 200 K, and their difference. (H) Temperature dependence of the total spectral intensity and the maximum peak height in the MDCs. Reproduced from [276]. CC BY 4.0.

plane is far from sufficient to confirm its altermagnetism. A comprehensive understanding of its three-dimensional spin polarization configuration is required.

3.6. $CoNb_4Se_8$

$CoNb_4Se_8$ crystallizes in the hexagonal space group $P6_3/mmc$ (No. 194) (figure 12(A)) and hosts a robust collinear antiferromagnetic order [274]. With the z-axis parallel to the crystal's c-axis, the two magnetic sublattices are thus related by a six-fold rotation C_{6z} combined with a 1/2 c translation, or alternatively, by the mirror M_z across the $c = 1/4$ plane, exhibiting altermagnetism. Through symmetry analysis and first-principles calculations, Regmi *et al* [274] and Sah *et al* [277] showed that M_z and C_{6z} symmetry inherent to the $P6_3/mmc$ space group protect spin degeneracy in the $k_z = 0$ plane for A-type AFM stacking configuration. These symmetries enforce spin-degenerate nodal lines along high-symmetry paths such as $\Gamma - M - K - \Gamma$, while this symmetry breaking lifts the spin degeneracy, where profound spin splitting can be seen along the low-symmetry $\Gamma' - M'$ path in the $k_z = \pi/2c$ plane, as shown in figure 12(B). Although SOC induces additional band splitting along the high-symmetry nodal planes, the underlying symmetry forbids any net spin polarization there. These results confirm that, despite including SOC in the calculations, the centrosymmetric lattice preserves Kramers degeneracy at $k_z = 0$. To further illustrate this, Sakhya *et al* [275] and Sah *et al* [277] computed the Fermi surfaces with and without SOC (figure 12(C)). The left panel ($k_z = 0$) shows complete spin degeneracy, consistent with the symmetry-protected nodal lines. In contrast, the right panel ($k_z = \pi/2c$) exhibits clear spin splitting and strong spin polarization along $\Gamma' - M'$, matching the band dispersions in figure 12(B). This comparison highlights that in such A-type antiferromagnets, spin splitting originates from symmetry breaking even without SOC-a hallmark of altermagnets.

Dale *et al* [276] measured ARPES spectra of $CoNb_4Se_8$ along the M''–Γ'–M' momentum cut (figure 12(D)), in agreement with many of the salient features of the tight-binding model. They selected a specific off-nodal plane to highlight the spin splitting of two electron pockets at the BZ edge, consistent with DFT results that show opposite spin splittings at M and M. Figure 12(D) provides a spin-resolved view to examine this alternating splitting around the M' and M'' points. EDCs at momentum k_1 exhibit significant spin polarization. In contrast, at momentum $k_2 = C_2(k_1) = C_{36}\ (k_1)$, the spin splitting is reversed. The summary in figure 12(D) directly illustrates this alternating spin-splitting pattern, providing key evidence of T-symmetric SML.

However, the presence of alternating C_{6z} spin splitting alone does not fully confirm altermagnetic order, as similar effects might result from conventional SOC mechanisms. Thus, temperature-dependent evidence in figures 12(E)–(H) further confirms an altermagnetic phase transition in $CoNb_4Se_8$, indicated by temperature-dependent changes in spin splitting within the electronic structure. In the low-energy ARPES spectra, two distinct spin-split electron pockets emerge below the Néel temperature (figure 12(E)). Above this temperature (figure 12(F)), the spectral weight near the Fermi level decreases uniformly across the BZ. The change in spectral density (figure 12(G)) suggests a phase transition, typically accompanied by symmetry breaking. At 13 K, the MDCs at the Fermi level, shown in figure 12(H), exhibit two peaks with nearly equal intensity. Above the Néel transition, both peaks decrease sharply in intensity.

Similar to materials like α-MnTe and CrSb, merely detecting band splitting associated with the magnetic transition temperature and verifying spin polarization on a fixed plane are insufficient to conclusively demonstrate their altermagnetic nature. Verifying T-symmetry breaking SML in bulk BZ by SpinARPES is necessary.

Notably, the surface [28, 150, 195, 294] and strain [38, 101, 105] can induce phase transition from antiferromagnet to altermagnet, or among altermagnetic types. On the one hand, several recent studies [28, 150, 195, 294] have focused on two-dimensional altermagnetic systems, centering on surfaces/interfaces and thin films. They break through the limitations of traditional bulk altermagnetism research, taking the surface functionalization of antiferromagnets and thin film systems as the main research platforms. The results show that 'symmetry breaking' is the core mechanism for the emergence and regulation of altermagnetism: by terminating antiferromagnets in specific directions, the bulk PT (parity-time) symmetry is broken while the magnetic compensation symmetry is preserved, leading to the emergence of altermagnetism on the surface. For most materials, only one surface orientation can retain altermagnetism (e.g. the (110) surface of α-MnTe and the (100) surface of $LaMnO_3$), while the others are 'blind surfaces'. Moreover, the spin splitting magnitude of surface states is basically consistent with that of the bulk. In addition, an external electric field can activate altermagnetism on blind surfaces. Although SOC only slightly modifies the spin splitting amplitude, it can induce new spin textures without destroying the core characteristics of altermagnetism.

On the other hand, some researches, based on symmetry analysis and first-principles calculations, have adopted strain as the core regulatory tool to achieve multi-dimensional optimization of altermagnetism. Chakraborty *et al* [38] used compressive strain to drive the transition from the monoclinic phase (antiferromagnetism) to the tetragonal phase (d-wave altermagnetism), accompanied by a metal-insulator transition in ReO_2. Belashchenko *et al* [296] induced a *g*-wave to *d*-wave transition via 1% in-plane shear strain, with the spin splitting gauge factor exceeding 30 in α-MnTe. León *et al* [105] tuned magnetic stability using biaxial strain—2% tensile strain enhanced altermagnetic splitting by 9%, while compressive strain beyond 2% drives the phase transition from antiferromagnetism to altermagnetism in $Ca_3Ru_2O_7$. Karetta *et al* [101] realized a *g*-wave to *d*-wave transition through four types of shear strain, with the spin splitter effect reaching 5% under 1% strain in CrSb. These studies demonstrate the potential of strain engineering in controllable preparation of altermagnets, which is compatible with thin-film epitaxial growth technology.

4. Guidelines to identify an ideal altermagnet

Traversing through all the altermagnetic candidates that have been experimentally investigated and confronting the controversies directly, we have learned that ARPES and particularly SpinARPES could provide critical evidence for the existence of altermagnetism. Yet, cautiousness, much more than currently manifested, is needed in practice to obtain reliable information. Below are several guidelines which we hope can be informative in experimental investigation of band structure and spin polarization of altermagnetism.

4.1. The incompetence of band splitting

Among the ARPES studies on altermagnetic candidates with unresolved controversies, we notice several works claiming observation of altermagnet-type band splitting, without demonstrating the spin polarization. While band splitting could be the consequences of exchange coupling, it is not necessarily associated with altermagnetism. In fact, besides the *C*-paired antiferromagnetic sublattice symmetry, there are plenty of symmetry operations connecting the sublattice which can give rise to band splitting with similar shape of altermagnetic type yet without spin polarization. While it is beyond the scope of this review to present the group theory analysis and specify the potential spin groups, we could still conduct a deductive reasoning. As shown in figure 13, altermagnetic lattices (figures 13(A) and (B)) have no *PT* or *tT* symmetry but the *CT* symmetry leads to *T*-symmetry breaking SML (figures 13(C) and (D)). Note these two lattices have opposite dipole orientations. This leads to spin polarized CECs with opposite spin polarization. Assuming these two lattices are assembled in such a way that globally the *PT* or *tT* symmetry is retained, then the corresponding CECs preserving the *T*-symmetry. In fact, the shape of the total CECs follows that of the component sublattices and can be viewed as the superposition of both CECs. This is to say, the total band structure shares the same band splitting with the component sublattices, but without spin polarization. One outstanding example of the above hypothesis is the so called 'hidden altermagnetism', which has recently been discussed in V_2Se_2O family of materials. Globally this material may have a G-type [182] antiferromagnetic structure and the bands are spin degenerated, with band splitting follows the shape of altermagnetism hosted by each component layer. We thus reach the conclusion that just band splitting is far from enough to demonstrate the altermagnetic order.

4.2. Reliable spin polarization

Among the SpinARPES works on altermagnetic band structure, it is known to all that the observed spin polarization is of low magnitude, which is in stark contrast to the SOC type spin polarization such as that of the topological surface states [297] or hidden spin polarization [254, 298, 299]. This is mainly the results of compensation from opposite spin polarization signal corresponding to antiferromagnetic domains with opposite Néel vector. The size of these antiferromagnetic domains may vary from 100 nanometers to 10 micrometers according to the x-ray photoemission electron microscopy study on α-MnTe [214], which is much smaller than most of the SpinARPES instrumental spatial resolution decided by the beam spot size. It is tempting to align the antiferromagnetic domains using a high magnetic field, yet such device is usually unavailable in photoemission instruments due to the concern of magnetization. Recently, it is proved that field cooling can prepare a single-domain state of α-MnTe [193].

The low magnitude of altermagnetic spin polarization poses a great challenge for SpinARPES to achieve reliable polarization information. On the one hand, SpinARPES technique is notorious for its

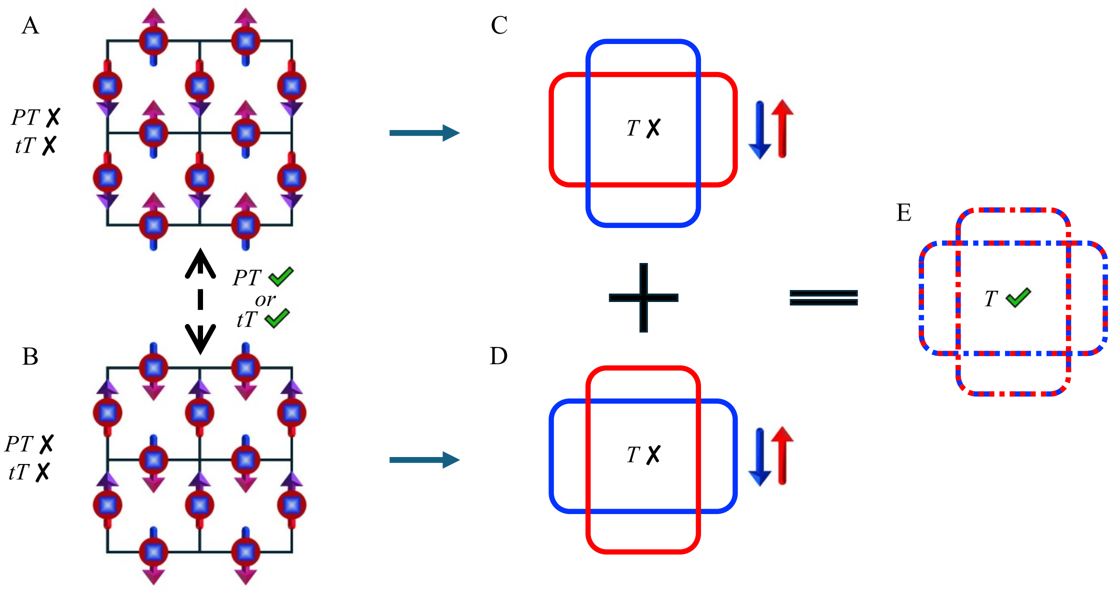

Figure 13. Schematic assembly of antiferromagnetic sublattices which possesses altermagnet-like band splitting without spin polarization. (A), (B) Constituents of antiferromagnetic sublattices. (C), (D) The corresponding spin polarized CECs. (E) The assembled spin degenerated CECs due to the contribution from both A and B components.

low efficiency. Unless a significant amount of time is spent for high level of signal statistic, spin polarization spectra are always suffering from noise since the polarization is defined as the difference between the counts from a pair of channeltrons divided by the sum of them. On the other hand, such noise is frequently found to be with the same level of magnitude as the band spin polarization of altermagnets. Consequently, it is vital to distinguish true band polarization signal from the noisy fluctuation. One must ensure the correspondence between the observed polarization feature and the spectral peak position/width in the measured energy/momentum distribution curves. Last but not the least, the measured spin polarization spectra should be repeatable, not only during the same measurement, but also for different pieces or positions of samples.

4.3. Spin–momentum locking

Besides reliable spin polarization features, one also need to make sure that the observed spin polarizations obey the altermagnetic symmetry in momentum space. As already been discussed in section 2, the SML in altermagnets can be either symmetric or antisymmetric in k_x–k_y momentum space depending on whether the spin degenerate nodal planes have z dependence. The bulk type SML, such as those show in figure 14(A) for bulk d-wave and in figure 14(C) for bulk g-wave, although has T-symmetry breaking SML in three-dimensional k_x–k_y–k_z space (figures 14(A1) and (C1)), would nevertheless manifest antisymmetric spin polarization in two-dimensional k_x–k_y space ($E(k_x,k_y,\uparrow) = E(-k_x,-k_y,\downarrow)$, figures 14(A2) and (C2)). This is also true for the planar type SML (figures 14(B) and (D)) if it is projected onto k_x–k_z space (figures 14(B3) and (D3)). In fact, such situation holds when the projected planes contain one less nodal planes than the bulk has. Consequently, it is vital to prove the symmetry of SML in both k_x–k_y and k_x–k_z space to verify the existence of bulk type altermagnetism.

Now let us consider the reality, from the aspects of ARPES measurement and candidate materials. In ARPES measurement, with a fixed photon energy one can detect the energy-momentum relation (dispersion) in a quasi-two-dimensional plane with determined k_z value. For altermagnets with planar type SML, such as RbV_2Te_2O family [192, 196], the T-symmetry breaking SML can be measured using one single photon energy ($E(k_x,k_y,\uparrow) = E(-k_x,-k_y,\uparrow)$ for any k_z). However, for altermagnets with bulk type SML, such as α-MnTe and CrSb, using one single photon energy one can only probe the antisymmetric spin polarization for a single k_z plane ($E(k_x,k_y,\uparrow) = E(-k_x,-k_y,\downarrow)$ at $k_z \neq 0$), which is not sufficient to prove the T-symmetry breaking SML expected for altermagnetism. Even worse, the SOC effect, which is quite strong in materials containing heavy elements such as in α-MnTe and CrSb, leads to k_z independent spin polarization in the presence of inversion symmetry breaking [195]. This SOC effect is ubiquitous at the surface of many altermagnetic candidates, making the observed antisymmetric SML not only insufficient to justify the altermagnetism, but also incapable of distinguishing bulk from surface effects.

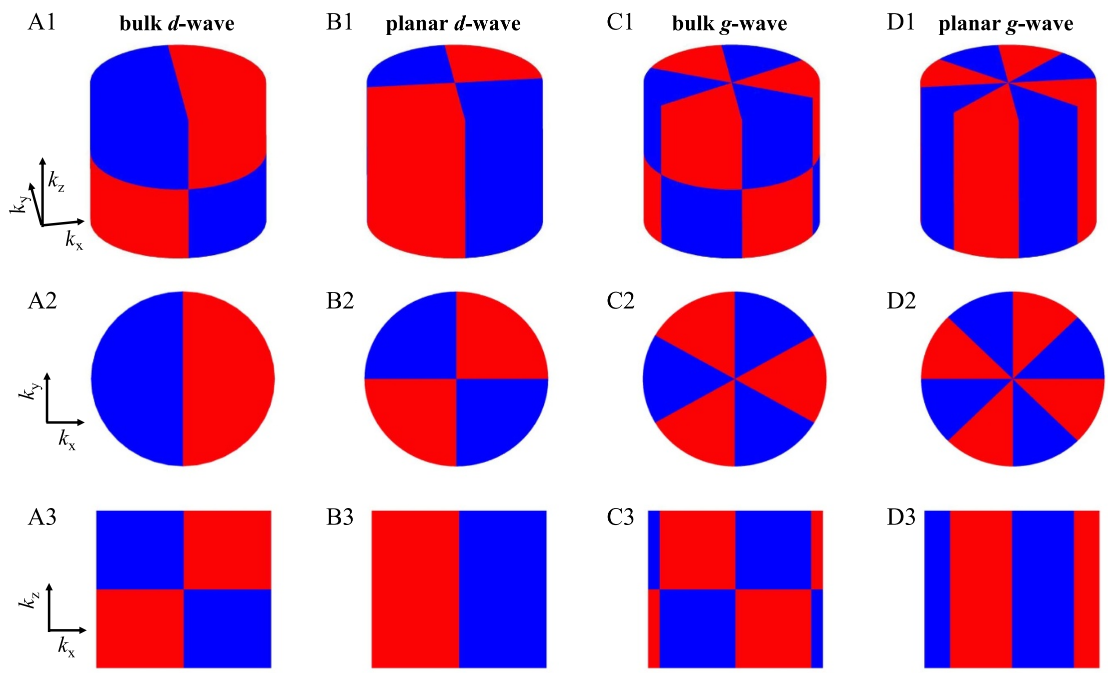

Figure 14. Schematic T-symmetry for planar and bulk type SML in three-dimensional $k_x - k_y - k_z$ space (A1)–(D1), the corresponding projection into $k_x - k_y$ space (A2)–(D2) and $k_x - k_z$ space (A3)–(D3). Blue and red colors indicate opposite spin polarizations.

It is thus essential to perform photon energy dependent SpinARPES measurements to establish the bulk type SML in altermagnets.

5. What characteristics should an ideal altermagnet have?

Having gone through all the workhorse altermagnetic candidates and particularly the controversies over many of them, one immediately realizes that many efforts are needed to explore reliable materials and their potential functionalities. Obviously, it is premature to draw any conclusion at the current stage. Instead, to possibly guide the material exploration and fulfill the tempting potential of altermagnetism, here we list several desirable characteristics which we prefer in an ideal altermagnet.

Layered structure enables exploration of various effects in two-dimensional materials that have been discovered in recent years, for example, the realization of topological superconductors via superconducting proximity effect [300], tunable electronic properties through gating [301, 302], modification of band structures through strain [303] and potential to form twisted systems like moiré superlattices [304]. Therefore, exploring layered materials in altermagnets is highly anticipated to realize more exotic states of matter and more promising potentials for developing high-density, high-speed and low-energy-consumption spintronic devices.

The functionality of altermagnets in spintronics typically relies on the pure spin currents or spin polarized currents. For example, in MRAMs, the strong spin polarization of the electrical current, provided by the ferromagnetic order, is used for both reading and writing. This asks for conductivity in the altermagnet-based MRAM development. Thus, metals or semiconductors are more favorable for altermagnetic candidates. Furthermore, while in principle altermagnets with all kind of spin symmetries can have TMR used in MRAM, the bulk conductivity of an altermagnet itself is spin dependent only in d-wave. Thus, a metallic, d-wave altermagnet is highly desired. Such expectation is recently realized in RbV_2Te_2O family [192, 196], yet it is chemically unstable in atmosphere due to the existence of alkali atoms. Further efforts are needed to achieve chemical stability in this material family, for an ultimate goal of realizing ideal altermagnet.

Acknowledgements

This work is supported by the Guangdong Major Project of Basic Research (Grant No. 2026B0303000004), National Key R&D Program of China (grant nos. 2025YFA1411200 and 2022YFA1403700), National Natural Science Foundation of China (grant no. 12574068,12474351), Guangdong Basic and Applied Basic Research Foundation (grant nos. 2022B1515020046, 2022B1515130005 and 2021B1515130007).

Data availability statement

All data that support the findings of this study are included within the article (and any supplementary files).

Author contributions

Xiangnan Xie
Writing – original draft (supporting)

Xiaoyue He
Writing – original draft (supporting)

Fayuan Zhang
Writing – review & editing (equal)

Chaoyu Chen 0000-0002-3930-8294
Conceptualization (lead), Writing – original draft (lead)

References

[1] Smejkal L, Gonzalez-Hernandez R, Jungwirth T and Sinova J 2020 Crystal time-reversal symmetry breaking and spontaneous Hall effect in collinear antiferromagnets *Sci. Adv.* **6** eaaz8809
[2] Hayami S, Yanagi Y and Kusunose H 2019 Momentum-dependent spin splitting by collinear antiferromagnetic ordering *J. Phys. Soc. Jpn.* **88** 123702
[3] Naka M, Hayami S, Kusunose H, Yanagi Y, Motome Y and Seo H 2019 Spin current generation in organic antiferromagnets *Nat. Commun.* **10** 4305
[4] Hayami S, Yanagi Y and Kusunose H 2020 Spontaneous antisymmetric spin splitting in noncollinear antiferromagnets without spin-orbit coupling *Phys. Rev. B* **101** 220403
[5] Hayami S, Yanagi Y and Kusunose H 2020 Bottom-up design of spin-split and reshaped electronic band structures in antiferromagnets without spin-orbit coupling: procedure on the basis of augmented multipoles *Phys. Rev. B* **102** 144441
[6] Yuan L-D, Wang Z, Luo J-W, Rashba E I and Zunger A 2020 Giant momentum-dependent spin splitting in centrosymmetric low-Z antiferromagnets *Phys. Rev. B* **102** 014422
[7] Gonzalez-Hernandez R, Šmejkal L, Výborný K, Yahagi Y, Sinova J, Jungwirth T and Železný J 2021 Efficient electrical spin splitter based on nonrelativistic collinear antiferromagnetism *Phys. Rev. Lett.* **126** 127701
[8] Ma H-Y, Hu M, Li N, Liu J, Yao W, Jia J-F and Liu J 2021 Multifunctional antiferromagnetic materials with giant piezomagnetism and noncollinear spin current *Nat. Commun.* **12** 2846
[9] Mazin I I, Koepernik K, Johannes M D, Gonzalez-Hernandez R and Smejkal L 2021 Prediction of unconventional magnetism in doped $FeSb_2$ *Proc. Natl Acad. Sci. USA* **118** e2108924118
[10] Yuan L-D, Wang Z, Luo J-W and Zunger A 2021 Prediction of low-Z collinear and noncollinear antiferromagnetic compounds having momentum-dependent spin splitting even without spin-orbit coupling *Phys. Rev. Mater.* **5** 014409
[11] Liu P, Li J, Han J, Wan X and Liu Q 2022 Spin-group symmetry in magnetic materials with negligible spin-orbit coupling *Phys. Rev. X* **12** 021016
[12] Mazin I 2022 Editorial: altermagnetism—a new punch line of fundamental magnetism *Phys. Rev. X* **12** 040002
[13] Naka M, Motome Y and Seo H 2022 Anomalous Hall effect in antiferromagnetic perovskites *Phys. Rev. B* **106** 195149
[14] Šmejkal L, Hellenes A B, González-Hernández R, Sinova J and Jungwirth T 2022 Giant and tunneling magnetoresistance in unconventional collinear antiferromagnets with nonrelativistic spin-momentum coupling *Phys. Rev. X* **12** 011028
[15] Šmejkal L, MacDonald A H, Sinova J, Nakatsuji S and Jungwirth T 2022 Anomalous Hall antiferromagnets *Nat. Rev. Mater.* **7** 482–96
[16] Šmejkal L, Sinova J and Jungwirth T 2022 Emerging research landscape of altermagnetism *Phys. Rev. X* **12** 040501
[17] Šmejkal L, Sinova J and Jungwirth T 2022 Beyond conventional ferromagnetism and antiferromagnetism: a phase with nonrelativistic spin and crystal rotation symmetry *Phys. Rev. X* **12** 031042
[18] Cui Q, Zhu Y, Yao X, Cui P and Yang H 2023 Giant spin-Hall and tunneling magnetoresistance effects based on a two-dimensional nonrelativistic antiferromagnetic metal *Phys. Rev. B* **108** 024410
[19] Mazin I I 2023 Altermagnetism in MnTe: origin, predicted manifestations, and routes to detwinning *Phys. Rev. B* **107** L100418
[20] Lovesey S W, Khalyavin D D and van der Laan G 2023 Templates for magnetic symmetry and altermagnetism in hexagonal MnTe *Phys. Rev. B* **108** 174437

[21] Guo Y, Liu H, Janson O, Fulga I C, van den Brink J and Facio J I 2023 Spin-split collinear antiferromagnets: a large-scale *ab-initio* study *Mater. Today Phys.* **32** 100991
[22] Hou X-Y, Yang H-C, Liu Z-X, Guo P-J and Lu Z-Y 2023 Large intrinsic anomalous Hall effect in both Nb2FeB2 and Ta2FeB2 with collinear antiferromagnetism *Phys. Rev. B* **107** L161109
[23] Jiang Y-Y, Wang Z-A, Samanta K, Zhang S-H, Xiao R-C, Lu W J, Sun Y P, Tsymbal E Y and Shao D-F 2023 Prediction of giant tunneling magnetoresistance in $RuO_2/TiO_2/RuO_2$ (110) antiferromagnetic tunnel junctions *Phys. Rev. B* **108** 174439
[24] Li Y-X and Liu C-C 2023 Majorana corner modes and tunable patterns in an altermagnet heterostructure *Phys. Rev. B* **108** 205410
[25] Mazin I, González-Hernández R and Šmejkal L 2023 Induced monolayer altermagnetism in MnP (S, Se)3 and FeSe (arXiv:2309.02355)
[26] Ouassou J A, Brataas A and Linder J 2023 dc Josephson effect in altermagnets *Phys. Rev. Lett.* **131** 076003
[27] Papaj M 2023 Andreev reflection at the altermagnet-superconductor interface *Phys. Rev. B* **108** L060508
[28] Sattigeri R M, Cuono G and Autieri C 2023 Altermagnetic surface states: towards the observation and utilization of altermagnetism in thin films, interfaces and topological materials *Nanoscale* **15** 16998–7005
[29] Šmejkal L *et al* 2023 Chiral magnons in altermagnetic RuO_2 *Phys. Rev. Lett.* **131** 256703
[30] Sun C, Brataas A and Linder J 2023 Andreev reflection in altermagnets *Phys. Rev. B* **108** 054511
[31] Yuan L-D, Zhang X, Acosta C M and Zunger A 2023 Uncovering spin-orbit coupling-independent hidden spin polarization of energy bands in antiferromagnets *Nat. Commun.* **14** 5301
[32] Zhu D, Zhuang Z-Y, Wu Z and Yan Z 2023 Topological superconductivity in two-dimensional altermagnetic metals *Phys. Rev. B* **108** 184505
[33] Andriy S, Libor Š and Igor I M 2024 A tool to check whether a symmetry-compensated collinear magnetic material is antiferro- or altermagnetic (arXiv:2401.08784)
[34] Devaraj N, Bose A and Narayan A 2024 Interplay of altermagnetism and pressure in hexagonal and orthorhombic MnTe *Phys. Rev. Mater.* **8** 104407
[35] Bai L, Feng W, Liu S, Šmejkal L, Mokrousov Y and Yao Y 2024 Altermagnetism: exploring new frontiers in magnetism and spintronics *Adv. Funct. Mater.* **34** 2409327
[36] Banerjee S and Scheurer M S 2024 Altermagnetic superconducting diode effect *Phys. Rev. B* **110** 024503
[37] Bhowal S and Spaldin N A 2024 Ferroically ordered magnetic octupoles in d-wave altermagnets *Phys. Rev. X* **14** 011019
[38] Chakraborty A, González Hernández R, Šmejkal L and Sinova J 2024 Strain-induced phase transition from antiferromagnet to altermagnet *Phys. Rev. B* **109** 144421
[39] Chakraborty D and Black-Schaffer A M 2024 Zero-field finite-momentum and field-induced superconductivity in altermagnets *Phys. Rev. B* **110** L060508
[40] Chen X *et al* 2024 Enumeration and representation theory of spin space groups *Phys. Rev. X* **14** 031038
[41] Cheng Q, Mao Y and Sun Q-F 2024 Field-free Josephson diode effect in altermagnet/normal metal/altermagnet junctions *Phys. Rev. B* **110** 014518
[42] Cheong S-W and Huang F-T 2024 Altermagnetism with non-collinear spins *npj Quantum Mater.* **9** 13
[43] Chi B, Jiang L, Zhu Y, Yu G, Wan C, Zhang J and Han X 2024 Crystal-facet-oriented altermagnets for detecting ferromagnetic and antiferromagnetic states by giant tunneling magnetoresistance *Phys. Rev. Appl.* **21** 034038
[44] Das S and Soori A 2024 Crossed Andreev reflection in altermagnets *Phys. Rev. B* **109** 245424
[45] Ezawa M 2024 Detecting the Neel vector of altermagnets in heterostructures with a topological insulator and a crystalline valley-edge insulator *Phys. Rev. B* **109** 245306
[46] Fang Y, Cano J and Ghorashi S A A 2024 Quantum geometry induced nonlinear transport in altermagnets *Phys. Rev. Lett.* **133** 106701
[47] Ghorashi S A A, Hughes T L and Cano J 2024 Altermagnetic routes to Majorana modes in zero net magnetization *Phys. Rev. Lett.* **133** 106601
[48] Giil H G and Linder J 2024 Superconductor-altermagnet memory functionality without stray fields *Phys. Rev. B* **109** 134511
[49] Gomonay O, Kravchuk V P, Jaeschke-Ubiergo R, Yershov K V, Jungwirth T, Šmejkal L, Brink J V D and Sinova J 2024 Structure, control, and dynamics of altermagnetic textures *npj Spintronics* **2** 35
[50] Gurung G, Elekhtiar M, Luo Q Q, Shao D F and Tsymbal E Y 2024 Nearly perfect spin polarization of noncollinear antiferromagnets *Nat. Commun.* **15** 10242
[51] He T, Li L, Cui C, Zhang R-W, Yu Z-M, Liu G and Zhang X 2024 Quasi-one-dimensional spin transport in altermagnetic Z3 nodal net metals *Phys. Rev. Lett.* **133** 146602
[52] Jaeschke-Ubiergo R, Bharadwaj V K, Jungwirth T, Šmejkal L and Sinova J 2024 Supercell altermagnets *Phys. Rev. B* **109** 094425
[53] Jiang Y *et al* 2024 Enumeration of spin-space groups: toward a complete description of symmetries of magnetic orders *Phys. Rev. X* **14** 031039
[54] Jin H, Tan Z, Gong Z and Wang J 2024 Anomalous Hall effect in two-dimensional vanadium tetrahalogen with altermagnetic phase *Phys. Rev. B* **110** 155125
[55] Jungwirth T, Fernandes R M, Sinova J and Smejkal L 2024 Altermagnets and beyond: nodal magnetically-ordered phases (arXiv:2409.10034)
[56] Leeb V, Mook A, Smejkal L and Knolle J 2024 Spontaneous formation of altermagnetism from orbital ordering *Phys. Rev. Lett.* **132** 236701
[57] Li J-Y, Fan A-D, Wang Y-K, Zhang Y and Li S 2024 Strain-induced valley polarization, topological states, and piezomagnetism in two-dimensional altermagnetic V_2Te_2O, V_2STeO, V_2SSeO, and V_2S_2O *Appl. Phys. Lett.* **125** 222404
[58] Li Y-X, Liu Y and Liu C-C 2024 Creation and manipulation of higher-order topological states by altermagnets *Phys. Rev. B* **109** L201109
[59] Liu Y, Li J, Liu P and Liu Q 2024 Unconventional spin textures emerging from a universal symmetry theory of spin-momentum locking *npj Quantum Mater.* **9** 69
[60] Liu Y, Yu J and Liu C C 2024 Twisted magnetic van der Waals bilayers: an ideal platform for altermagnetism *Phys. Rev. Lett.* **133** 206702
[61] Lu B, Maeda K, Ito H, Yada K and Tanaka Y 2024 phi Josephson junction induced by altermagnetism *Phys. Rev. Lett.* **133** 226002
[62] Ma H-Y and Jia J-F 2024 Altermagnetic topological insulator with C-paired spin-valley locking *Quantum Frontiers* **3** 22
[63] Mazin I 2024 Altermagnetism then and now *Physics* **17** 4
[64] McClarty P A and Rau J G 2024 Landau theory of altermagnetism *Phys. Rev. Lett.* **132** 176702

[65] Sato T, Haddad S, Fulga I C, Assaad F F and van den Brink J 2024 Altermagnetic anomalous Hall effect emerging from electronic correlations *Phys. Rev. Lett.* **133** 086503
[66] Smolyanyuk A, Mazin I I, Garcia-Gassull L and Valentí R 2024 Fragility of the magnetic order in the prototypical altermagnet RuO_2 *Phys. Rev. B* **109** 134424
[67] Sødequist J and Olsen T 2024 Two-dimensional altermagnets from high throughput computational screening: symmetry requirements, chiral magnons, and spin-orbit effects *Appl. Phys. Lett.* **124** 182409
[68] Weber M *et al* 2024 Ultrafast electron dynamics in altermagnetic materials (arXiv:2411.08160)
[69] Weber S F, Urru A, Bhowal S, Ederer C and Spaldin N A 2024 Surface magnetization in antiferromagnets: classification, example materials, and relation to magnetoelectric responses *Phys. Rev. X* **14** 021033
[70] Wei C-C, Lawrence E, Tran A and Ji H 2024 Crystal chemistry and design principles of altermagnets *ACS Org. Inorg. Au.* **4** 604–19
[71] Xiao Z, Zhao J, Li Y, Shindou R and Song Z-D 2024 Spin space groups: full classification and applications *Phys. Rev. X* **14** 031037
[72] Yan H, Zhou X, Qin P and Liu Z 2024 Review on spin-split antiferromagnetic spintronics *Appl. Phys. Lett.* **124** 030503
[73] Yuan L-D, Georgescu A B and Rondinelli J M 2024 Nonrelativistic spin splitting at the Brillouin zone center in compensated magnets *Phys. Rev. Lett.* **133** 216701
[74] Zeng S and Zhao Y-J 2024 Description of two-dimensional altermagnetism: categorization using spin group theory *Phys. Rev. B* **110** 054406
[75] Zeng S and Zhao Y-J 2024 Bilayer stacking A-type altermagnet: a general approach to generating two-dimensional altermagnetism *Phys. Rev. B* **110** 174410
[76] Zhang S-B, Hu L-H and Neupert T 2024 Finite-momentum Cooper pairing in proximitized altermagnets *Nat. Commun.* **15** 1801
[77] Zhu Y, Chen T, Li Y, Qiao L, Ma X, Liu C, Hu T, Gao H and Ren W 2024 Multipiezo effect in altermagnetic V_2SeTeO monolayer *Nano Lett.* **24** 472–8
[78] Autieri C, Cuono G, Chakraborty D, Gentile P and Black-Schaffer A M 2025 Conditions for orbital-selective altermagnetism in Sr_2RuO_4: tight-binding model, similarities with cuprates, and implications for superconductivity *Phys. Rev. B* **112** 014412
[79] Autieri C, Sattigeri R M, Cuono G and Fakhredine A 2025 Staggered Dzyaloshinskii-Moriya interaction inducing weak ferromagnetism in centrosymmetric altermagnets and weak ferrimagnetism in noncentrosymmetric altermagnets *Phys. Rev. B* **111** 054442
[80] Bhattarai R, Minch P and Rhone T D 2025 High-throughput screening of altermagnetic materials *Phys. Rev. Mater.* **9** 064403
[81] Che Y, Lv H, Wu X and Yang J 2025 Engineering altermagnetic states in two-dimensional square tessellations *Phys. Rev. Lett.* **135** 036701
[82] Chen W, Zhou X, Lou W-K and Chang K 2025 Magneto-optical conductivity and circular dichroism in d-wave altermagnets *Phys. Rev. B* **111** 064428
[83] Chen X, Liu Y, Liu P, Yu Y, Ren J, Li J, Zhang A and Liu Q 2025 Unconventional magnons in collinear magnets dictated by spin space groups *Nature* **640** 349–54
[84] Duan X, Zhang J, Zhu Z, Liu Y, Zhang Z, Žutić I and Zhou T 2025 Antiferroelectric altermagnets: antiferroelectricity alters magnets *Phys. Rev. Lett.* **134** 106801
[85] Fan Z, Zhang Z, Wang H, Gong J, Wang D and Wang B 2025 High-pressure modulation of altermagnetism in MnF_2 *Appl. Phys. Lett.* **126** 082409
[86] Farajollahpour T, Ganesh R and Samokhin K V 2025 Light-induced charge and spin Hall currents in materials with C4K symmetry *npj Quantum Mater.* **10** 24
[87] Fukaya Y, Maeda K, Yada K, Cayao J, Tanaka Y and Lu B 2025 Josephson effect and odd-frequency pairing in superconducting junctions with unconventional magnets *Phys. Rev. B* **111** 064502
[88] Gao Z-F, Qu S, Zeng B, Liu Y, Wen J-R, Sun H, Guo P-J and Lu Z-Y 2025 AI-accelerated discovery of altermagnetic materials *Natl Sci. Rev.* **12** nwaf066
[89] Gauswami A and Jha P K 2025 Exploration of surface oriented altermagnetic states in CrTe, $FeSb_2$and MnO_2: a first-principles study *J. Phys: Condens. Matter* **37** 305801
[90] González-Hernández R, Serrano H and Uribe B 2025 Spin Chern number in altermagnets *Phys. Rev. B* **111** 085127
[91] Guo S-D 2025 Hidden altermagnetism *Front. Phys.* **21** 025201
[92] Guo S-D 2025 Hidden fully-compensated ferrimagnetism *Phys. Chem. Chem. Phys.* **28** 2188–94
[93] Ho D Q, To D Q, Hu R, Bryant G W and Janotti A 2025 Symmetry-breaking induced surface magnetization in nonmagnetic RuO_2 *Phys. Rev. Mater.* **9** 094406
[94] Hoyer R, Stavropoulos P P, Razpopov A, Valentí R, Šmejkal L and Mook A 2025 Altermagnetic splitting of magnons in hematite $\alpha-Fe_2O_3$ *Phys. Rev. B* **112** 064425
[95] Hu J X, Matsyshyn O and Song J C W 2025 Nonlinear superconducting magnetoelectric effect *Phys. Rev. Lett.* **134** 026001
[96] Hu M, Cheng X, Huang Z and Liu J 2025 Catalog of C-paired spin-momentum locking in antiferromagnetic systems *Phys. Rev. X* **15** 021083
[97] Hu M, Janson O, Felser C, McClarty P, van den Brink J and Vergniory M G 2025 Spin Hall and Edelstein effects in chiral non-collinear altermagnets *Nat. Commun.* **16** 8529
[98] Jaeschke-Ubiergo R *et al* 2025 Atomic altermagnetism (arXiv:2503.10797)
[99] Jungwirth T, Fernandes R M, Fradkin E, MacDonald A H, Sinova J and Šmejkal L 2025 Altermagnetism: an unconventional spin-ordered phase of matter *Newton* **1** 100162
[100] Jungwirth T *et al* 2025 Altermagnetic spintronics (arXiv:2508.09748)
[101] Karetta B, Verbeek X H, Jaeschke-Ubiergo R, Šmejkal L and Sinova J 2025 Strain-controlled g- to d-wave transition in altermagnetic CrSb *Phys. Rev. B* **112** 094454
[102] Khan I, Bezzerga D, Marfoua B and Hong J 2025 Altermagnetism, piezovalley, and ferroelectricity in two-dimensional Cr_2SeO altermagnet *npj 2D Mater. Appl.* **9** 18
[103] Krüger P 2025 Circular dichroism in resonant photoelectron diffraction as a direct probe of sublattice magnetization in altermagnets *Phys. Rev. Lett.* **135** 196703
[104] Larionov K V and Sorokin P B 2025 Trace of altermagnetism in GdAlSi films: towards the 2D limit *J. Mater. Chem. C* **13** 8665–70
[105] León A, Autieri C, Brumme T and González J W 2025 Hybrid d/p-wave altermagnetism in $Ca_3Ru_2O_7$ and strain-controlled spin splitting *npj Quantum Mater.* **10** 98

[106] Li J-Y, Fan A-D, Li S and Yang W-L 2025 Optical dichroism, valley polarization, and noncollinear spin currents in monolayer altermagnetic Ca(CoN)$_2$ *Appl. Phys. Lett.* **127** 131901

[107] Li S, Zhang Y, Bahri A, Zhang X and Jia C 2025 Altermagnetism and strain induced altermagnetic transition in Cairo pentagonal monolayer *npj Quantum Mater.* **10** 83

[108] Li Y, Leeb V, Wohlfeld K, Valentí R and Knolle J 2025 Exploring d-wave magnetism in cuprates from oxygen moments *Phys. Rev. B* **112** 125139

[109] Li Y-X *et al* 2025 Exploration of altermagnetism in RuO$_2$ (arXiv:2509.19932)

[110] Li Z, Li Z and Qiao Z 2025 Altermagnetism-induced topological phase transitions in the Kane-Mele model *Phys. Rev. B* **111** 155303

[111] Liu C, Li X, Li X and Yang J 2025 Realizing abundant two-dimensional altermagnets with anisotropic spin current via spatial inversion symmetry breaking *Nano Lett.* **25** 9197–203

[112] Liu D, Zeng S, Liao J-H and Zhao Y-J 2025 Unlocking altermagnetism in antiferromagnetic 2D films via adsorption (arXiv:2507.09518)

[113] Liu Q, Dai X and Blügel S 2025 Different facets of unconventional magnetism *Nat. Phys.* **21** 329–31

[114] Liu Z, Hu H and Liu X-J 2025 Altermagnetism and superconductivity: a short historical review (arXiv:2510.09170)

[115] Naka M, Motome Y and Seo H 2025 Altermagnetic perovskites *npj Spintronics* **3** 1

[116] Parfenov O E, Averyanov D V, Sokolov I S, Mihalyuk A N, Kondratev O A, Taldenkov A N, Tokmachev A M and Storchak V G 2025 Pushing an altermagnet to the ultimate 2D limit: symmetry breaking in monolayers of GdAlSi *J. Am. Chem. Soc.* **147** 5911–20

[117] Parfenov O E, Averyanov D V, Sokolov I S, Mihalyuk A N, Kondratev O A, Taldenkov A N, Tokmachev A M and Storchak V G 2025 Scaling the altermagnet GdAlSi beyond the monolayer limit *J. Am. Chem. Soc.* **147** 23857–67

[118] Peng H, Zeng S, Liao J-H, He C-C, Yang X-B and Zhao Y-J 2025 Multicomponent altermagnet: a general approach to generating multicomponent structures with two-dimensional altermagnetism *Phys. Rev. B* **111** 195123

[119] Qian Z, Yang Y, Liu S and Wu C 2025 Fragile unconventional magnetism in RuO$_2$ by proximity to Landau-Pomeranchuk instability *Phys. Rev. B* **111** 174425

[120] Qu S, Hou X-Y, Liu Z-X, Guo P-J and Lu Z-Y 2025 Altermagnetic Weyl node-network metals protected by spin symmetry *Phys. Rev. B* **111** 195138

[121] Raghuvanshi P R *et al* 2025 Altermagnetic behavior in OsO2: parallels with RuO$_2$ *Phys. Rev. Mater.* **9** 034407

[122] Rathore D A 2025 Symmetry-driven spin splitting and its role in spintronic technologies *J. Alloys Compd.* **1034** 181292

[123] Roig M, Yu Y, Ekman R C, Kreisel A, Andersen B M and Agterberg D F 2025 Quasisymmetry-constrained spin ferromagnetism in altermagnets *Phys. Rev. Lett.* **135** 016703

[124] Smolyanyuk A, Šmejkal L and Mazin I I 2025 Origin of the anomalous Hall effect in Cr-doped RuO$_2$ *Phys. Rev. B* **111** 064406

[125] Song C, Bai H, Zhou Z, Han L, Reichlova H, Dil J H, Liu J, Chen X and Pan F 2025 Altermagnets as a new class of functional materials *Nat. Rev. Mater.* **10** 473–85

[126] Sun H, Zhang Z, Liu K, Du Y, Sun L and Zhao M 2025 Highly anisotropic spin plasmons in two-dimensional altermagnetic materials *Phys. Rev. B* **112** 115413

[127] Tamang R, Gurung S, Rai D P, Brahimi S and Lounis S 2025 Altermagnetism and altermagnets: a brief review *Magnetism* **5** 17

[128] Tenzin K, Kilic B, Sattigeri R M, He Z, Ye C C, Costa M, Nardelli M B, Autieri C and Sławińska J 2025 Persistent spin textures, altermagnetism and charge-to-spin conversion in metallic chiral crystals TM(3)X(6) *npj Spintronics* **3** 46

[129] Vila M, Sunko V and Moore J E 2025 Orbital-spin locking and its optical signatures in altermagnets *Phys. Rev. B* **112** L020401

[130] Wan X, Mandal S, Guo Y and Haule K 2025 High-throughput search for metallic altermagnets by embedded dynamical mean field theory *Phys. Rev. Lett.* **135** 106501

[131] Wang D, Wang H, Liu L, Zhang J and Zhang H 2025 Electric-field-induced switchable two-dimensional altermagnets *Nano Lett.* **25** 498–503

[132] Wang S, Wang W-W, Fan J, Zhou X, Li X-P and Wang L 2025 Two-dimensional dual-switchable ferroelectric altermagnets: altering electrons and magnons *Nano Lett.* **25** 14618–24

[133] Wang X *et al* 2025 Layer Hall and layer spin Hall effects in two-dimensional altermagnets induced by spin-layer coupling *Phys. Rev. B* **112** 134421

[134] Wang Z-M, Zhang Y, Zhang S-B, Sun J-H, Dagotto E, Xu D-H and Hu L-H 2025 Spin-orbital altermagnetism *Phys. Rev. Lett.* **135** 176705

[135] Weber M, Leckron K, Haag L F, Jaeschke-Ubiergo R, Šmejkal L, Sinova J and Schneider H C 2025 Ultrafast electron dynamics in a planar d-wave altermagnet *Newton* **1** 100266

[136] Wenzel M, Uykur E, Rößler S, Schmidt M, Janson O, Tiwari A, Dressel M and Tsirlin A A 2025 Fermi-liquid behavior of nonaltermagnetic RuO$_2$ *Phys. Rev. B* **111** L041115

[137] Xu X and Yang L 2025 Alterpiezoresponse in two-dimensional Lieb-lattice altermagnets *Nano Lett.* **25** 11870–7

[138] Xun W, Liu X, Zhang Y, Wu Y-Z and Li P 2025 Stacking-, strain-engineering induced altermagnetism, multipiezo effect, and topological state in two-dimensional materials *Appl. Phys. Lett.* **126** 161903

[139] Zhan J-Y, He R, Wang D, He M-D, Luo N, Zeng J, Chen K-Q and Tang L-M 2025 Multiphysics field driven valley polarization in tetragonal altermagnets *Phys. Rev. B* **112** 024408

[140] Zhang S-S *et al* 2025 X-type stacking in cross-chain antiferromagnets *Newton* **1** 100068

[141] Zhang W *et al* 2025 Strain-induced nonrelativistic altermagnetic spin splitting effect *Phys. Rev. B* **112** 024415

[142] Zhang W, Zhu E, Li Z and Lv H 2025 Strain-tunable spin-valley locking and the influence of spin-orbit coupling in the two-dimensional altermagnet V_2Te_2O *Phys. Rev. B* **112** 144427

[143] Zhang Y-F, Ni X-S, Chen K and Cao K 2025 Chiral magnon splitting in altermagnetic CrSb from first principles *Phys. Rev. B* **111** 174451

[144] Zhou P, Peng X N, Hu Y Z, Pan B R, Liu S M, Lyu P B and Sun L Z 2025 Transition from antiferromagnets to altermagnets: symmetry-breaking theory *Phys. Rev. B* **112** 144419

[145] Zhu Z, Duan X, Zhang J, Hao B, Žutić I and Zhou T 2025 Two-dimensional ferroelectric altermagnets: from model to material realization *Nano Lett.* **25** 9456–62

[146] Zhu Z, Liu Y, Duan X, Zhang J, Hao B, Wei S-H, Žutić I and Zhou T 2025 Emergent multiferroic altermagnets and spin control via noncollinear molecular polarization *Sci. China: Phys. Mech. Astron.* **68** 127562

[147] Zou K *et al* 2025 Monolayer M2X2O as potential 2D altermagnets and half-metals: a first principles study *J. Phys: Condens. Matter* **37** 055804

[148] Autieri C and Fakhredine A 2026 Relativistic spin-momentum locking in altermagnets *J. Phys. Chem. Lett.* **17** 449–55
[149] Jungwirth T, Sinova J, Fernandes R M, Liu Q, Watanabe H, Murakami S, Nakatsuji S and Šmejkal L 2026 Symmetry, microscopy and spectroscopy signatures of altermagnetism *Nature* **649** 837–47
[150] Lange C *et al* 2026 Emergent altermagnetism at surfaces of antiferromagnets: full symmetry classification and material identification (arXiv:2602.08773)
[151] Li Y and Liu C-C 2026 Quantum-metric-based optical selection rules *Phys. Rev. Lett.* **136** 046901
[152] Thapa B, Chang P-H, Belashchenko K and Mazin I I 2026 Is altermagnetism in vanadium oxychalcogenides a lost cause? (arXiv:2602.18672)
[153] Tsirlin A A, Uykur E and Janson O 2026 Is ruthenium dioxide altermagnet? *Natl Sci. Rev.* nwag032
[154] Xu R, Gao Y and Liu J 2026 Chemical design of monolayer altermagnets *Natl Sci. Rev.* **13** nwaf528
[155] Awana G *et al* 2022 Critical analysis of proximity-induced magnetism in MnTe/Bi_2Te_3 heterostructures *Phys. Rev. Mater.* **6** 053402
[156] Li S *et al* 2022 Antiferromagnetic α-MnTe: molten-salt-assisted chemical vapor deposition growth and magneto-transport properties *Chem. Mater.* **34** 873–80
[157] Zhang Z, Dong X, Gao Z, Chen J, Wang B, Fu H, Du Y, Luo F and Wu J 2022 Ferromagnetic order in semiconducting Cr-doped α-MnTe nanosheets grown by chemical vapor deposition *Adv. Electron. Mater.* **8** 2200451
[158] Nie J H, Xie T, Chen G, Zhang W and Fu Y S 2023 Moire enhanced two-band superconductivity in a MnTe/$NbSe_2$ heterojunction *Nano Lett.* **23** 8370–7
[159] Wang T, Sun F, Hong W, Jian C, Ju Q, He X, Cai Q and Liu W 2023 Growth modulation of nonlayered 2D-MnTe and MnTe/WS2 heterojunctions for high-performance photodetectors *J. Mater. Chem. C* **11** 1464–9
[160] Bey S *et al* 2024 Unexpected tuning of the anomalous Hall effect in altermagnetic MnTe thin films (arXiv:2409.04567)
[161] Chilcote M *et al* 2024 Stoichiometry-induced ferromagnetism in altermagnetic candidate MnTe *Adv. Funct. Mater.* **34** 2405829
[162] Grzybowski M J *et al* 2024 Wurtzite vs. rock-salt MnSe epitaxy: electronic and altermagnetic properties *Nanoscale* **16** 6259–67
[163] Jain D, Yi H T, Mazza A R, Kisslinger K, Han M-G, Brahlek M and Oh S 2024 Buffer-layer-controlled nickeline vs zinc-blende/wurtzite-type MnTe growths on c-plane Al_2O_3 substrates *Phys. Rev. Mater.* **8** 014203
[164] Nag J *et al* 2024 GdAlSi: an antiferromagnetic topological Weyl semimetal with nonrelativistic spin splitting *Phys. Rev. B* **110** 224436
[165] Cuxart M G *et al* 2025 Emergent magnetic structures at the 2D limit of the altermagnet MnTe (arXiv:2504.11231)
[166] Lin W *et al* 2025 Tailoring altermagnetic spin splitting via strain-induced symmetry reconstruction in CrSb thin films *Adv. Mater.* **38** e15712
[167] Tseng C-H, Karube S, Shiota Y, Hisatomi R, Kan D, Shimakawa Y and Ono T 2025 Epitaxial growth of altermagnet CrSb via magnetron sputtering *Cryst. Growth Des.* **25** 9171–7
[168] Li K *et al* 2025 Two-dimensional altermagnetism in epitaxial CrSb ultrathin films (arXiv:2510.12344)
[169] Zhao G *et al* 2026 Pressure-induced metal-insulator and paramagnet-altermagnet transitions in rutile OsO2 single crystals *Newton* **2** 100441
[170] Kriegner D *et al* 2017 Magnetic anisotropy in antiferromagnetic hexagonal MnTe *Phys. Rev. B* **96** 214418
[171] Berlijn T *et al* 2017 Itinerant antiferromagnetism in RuO_2 *Phys. Rev. Lett.* **118** 077201
[172] Zhu Z H *et al* 2019 Anomalous antiferromagnetism in metallic RuO_2 determined by resonant x-ray scattering *Phys. Rev. Lett.* **122** 017202
[173] Lovesey S W, Khalyavin D D and van der Laan G 2022 Magnetic properties of RuO_2 and charge-magnetic interference in Bragg diffraction of circularly polarized x-rays *Phys. Rev. B* **105** 014403
[174] Biniskos N, Dos Santos F J, Schmalzl K, Raymond S, Dos Santos Dias M, Persson J, Marzari N, Blügel S, Lounis S and Brückel T 2022 Complex magnetic structure and spin waves of the noncollinear antiferromagnet Mn_5Si_3 *Phys. Rev. B* **105** 104404
[175] Wang P *et al* 2022 Concurrent pressure-induced spin-state transitions and Jahn–Teller distortions in MnTe *Chem. Mater.* **34** 3931–40
[176] Moseley D H *et al* 2022 Giant doping response of magnetic anisotropy in MnTe *Phys. Rev. Mater.* **6** 014404
[177] Kounta I *et al* 2023 Competitive actions of MnSi in the epitaxial growth of Mn_5Si_3 thin films on Si(111) *Phys. Rev. Mater.* **7** 024416
[178] Hiraishi M, Okabe H, Koda A, Kadono R, Muroi T, Hirai D and Hiroi Z 2024 Nonmagnetic ground state in RuO_2 revealed by muon spin rotation *Phys. Rev. Lett.* **132** 166702
[179] Keßler P *et al* 2024 Absence of magnetic order in RuO_2: insights from μSR spectroscopy and neutron diffraction *npj Spintronics* **2** 50
[180] Wang Z *et al* 2025 Atomic-scale spin sensing of a 2D d-wave altermagnet via helical tunneling (arXiv:2512.23290)
[181] Zhang Y-C *et al* 2025 Probing the Néel order in altermagnetic RuO_2 films by x-ray magnetic linear dichroism *Chin. Phys. Lett.* **42** 027301
[182] Sun Y *et al* 2025 Antiferromagnetic structure of KV_2Se_2O: a neutron diffraction study *Phys. Rev. B* **112** 184416
[183] Krempasky J *et al* 2024 Altermagnetic lifting of Kramers spin degeneracy *Nature* **626** 517–22
[184] Hajlaoui M *et al* 2024 Temperature dependence of relativistic valence band splitting induced by an altermagnetic phase transition *Adv. Mater.* **36** 2314076
[185] Reimers S *et al* 2024 Direct observation of altermagnetic band splitting in CrSb thin films *Nat. Commun.* **15** 2116
[186] Lee S *et al* 2024 Broken Kramers degeneracy in altermagnetic MnTe *Phys. Rev. Lett.* **132** 036702
[187] Zeng M *et al* 2024 Observation of spin splitting in room-temperature metallic antiferromagnet CrSb *Adv. Sci.* **11** e2406529
[188] Osumi T, Souma S, Aoyama T, Yamauchi K, Honma A, Nakayama K, Takahashi T, Ohgushi K and Sato T 2024 Observation of a giant band splitting in altermagnetic MnTe *Phys. Rev. B* **109** 115102
[189] Fedchenko O *et al* 2024 Observation of time-reversal symmetry breaking in the band structure of altermagnetic RuO_2 *Sci. Adv.* **10** eadj4883
[190] Liu J *et al* 2024 Absence of altermagnetic spin splitting character in rutile oxide RuO_2 *Phys. Rev. Lett.* **133** 176401
[191] Ding J *et al* 2024 Large band splitting in g-wave altermagnet CrSb *Phys. Rev. Lett.* **133** 206401
[192] Zhang F *et al* 2025 Crystal-symmetry-paired spin–valley locking in a layered room-temperature metallic altermagnet candidate *Nat. Phys.* **21** 760–7
[193] Din A D *et al* 2025 Unconventional relativistic spin polarization of electronic bands in an altermagnet (arXiv:2511.01690)
[194] Lee J-E, Zhong Y, Li Q, Edmonds M T, Shen Z-X, Hwang C and Mo S-K 2025 Dichotomous temperature response in the electronic structure of epitaxially grown altermagnet MnTe *Nano Lett.* **25** 8969–75

[195] Zeng M *et al* 2025 Non-altermagnetic spin texture in MnTe (arXiv:2511.02447)
[196] Jiang B *et al* 2025 A metallic room-temperature d-wave altermagnet *Nat. Phys.* **21** 754–9
[197] Yang G *et al* 2025 Observation of hidden altermagnetism in Cs1-δV_2Te_2O (arXiv:2512.00972)
[198] Lin Z *et al* 2025 Bulk band structure of RuO_2 measured with soft x-ray angle-resolved photoemission spectroscopy *Phys. Rev. B* **111** 134450
[199] Li C *et al* 2025 Topological Weyl altermagnetism in CrSb *Commun. Phys.* **8** 311
[200] Liao S *et al* 2025 Direct observation of large altermagnetic splitting in CrSb (100) thin film *Chin. Phys. Lett.* **42** 067503
[201] Lu W *et al* 2025 Signature of topological surface bands in altermagnetic Weyl semimetal CrSb *Nano Lett.* **25** 7343–50
[202] Yang G *et al* 2025 Three-dimensional mapping of the altermagnetic spin splitting in CrSb *Nat. Commun.* **16** 1442
[203] Karube S, Tanaka T, Sugawara D, Kadoguchi N, Kohda M and Nitta J 2022 Observation of spin-splitter torque in collinear antiferromagnetic RuO_2 *Phys. Rev. Lett.* **129** 137201
[204] Bose A *et al* 2022 Tilted spin current generated by the collinear antiferromagnet ruthenium dioxide *Nat. Electron.* **5** 267–74
[205] Bai H *et al* 2022 Observation of spin splitting torque in a collinear antiferromagnet RuO_2 *Phys. Rev. Lett.* **128** 197202
[206] Bai H *et al* 2023 Efficient spin-to-charge conversion via altermagnetic spin splitting effect in antiferromagnet RuO_2 *Phys. Rev. Lett.* **130** 216701
[207] Liu Y, Bai H, Song Y, Ji Z, Lou S, Zhang Z, Song C and Jin Q 2023 Inverse altermagnetic spin splitting effect-induced terahertz emission in RuO_2 *Adv. Opt. Mater.* **11** 2300177
[208] Zhang Y, Bai H, Han L, Chen C, Zhou Y, Back C H, Pan F, Wang Y and Song C 2024 Simultaneous high charge-spin conversion efficiency and large spin diffusion length in altermagnetic RuO_2 *Adv. Funct. Mater.* **34** 2313332
[209] Guo Y *et al* 2024 Direct and inverse spin splitting effects in altermagnetic RuO_2 *Adv. Sci.* **11** e2400967
[210] Liao C T, Wang Y C, Tien Y C, Huang S Y and Qu D 2024 Separation of inverse altermagnetic spin-splitting effect from inverse spin Hall effect in RuO_2 *Phys. Rev. Lett.* **133** 056701
[211] Li Z *et al* 2025 Fully field-free spin-orbit torque switching induced by spin splitting effect in altermagnetic RuO_2 *Adv. Mater.* **37** 2416712
[212] Aoyama T and Ohgushi K 2024 Piezomagnetic properties in altermagnetic MnTe *Phys. Rev. Mater.* **8** L041402
[213] Hariki A *et al* 2024 X-ray magnetic circular dichroism in altermagnetic α-MnTe *Phys. Rev. Lett.* **132** 176701
[214] Amin O J *et al* 2024 Nanoscale imaging and control of altermagnetism in MnTe *Nature* **636** 348–53
[215] Sasabe N, Mizumaki M, Uozumi T and Yamasaki Y 2023 Ferroic order for anisotropic magnetic dipole term in collinear antiferromagnets of (t2g)4 system *Phys. Rev. Lett.* **131** 216501
[216] Yamasaki Y, Ishii Y and Sasabe N 2025 Sum rules for x-ray circular and linear dichroism based on complete magnetic multipole basis *Sci. Technol. Adv. Mater.* **26** 2513217
[217] Hariki A, Takahashi Y and Kuneš J 2024 x-ray magnetic circular dichroism in RuO_2 *Phys. Rev. B* **109** 094413
[218] Hariki A, Okauchi T, Takahashi Y and Kuneš J 2024 Determination of the néel vector in rutile altermagnets through x-ray magnetic circular dichroism: the case of MnF_2 *Phys. Rev. B* **110** L100402
[219] Hariki A, Sakurai K, Okauchi T and Kuneš J 2025 Separating altermagnetic and ferromagnetic effects in x-ray magnetic dichroism of rutile NiF_2 *npj Quantum Mater.* **10** 49
[220] Li W, Li W, Zou M, Yin Y, Li H, Qu G, Huang Y, Yu R, Yang H and Wang B 2025 Large anisotropic x-ray magnetic circular dichroism in altermagnetic CrSb with collinear antiferromagnetic structure at room temperature *Phys. Rev. B* **111** 224417
[221] Takegami D *et al* 2025 Circular dichroism in resonant inelastic x-ray scattering: probing altermagnetic domains in MnTe *Phys. Rev. Lett.* **135** 196502
[222] Yamamoto R *et al* 2025 Altermagnetic nanotextures revealed in bulk MnTe *Phys. Rev. Appl.* **24** 034037
[223] Biniskos N, Dos Santos Dias M, Agrestini S, Sviták D, Zhou K-J, Pospíšil J and Čermák P 2025 Systematic mapping of altermagnetic magnons by resonant inelastic x-ray circular dichroism *Nat. Commun.* **16** 9311
[224] Yu T, Shahid I, Liu P, Shao D-F, Chen X-Q and Sun Y 2025 Néel vector-dependent anomalous transport in altermagnetic metal CrSb *npj Quantum Mater.* **10** 47
[225] Feng Z *et al* 2022 An anomalous Hall effect in altermagnetic ruthenium dioxide *Nat. Electron.* **5** 735–43
[226] Wang M *et al* 2023 Emergent zero-field anomalous Hall effect in a reconstructed rutile antiferromagnetic metal *Nat. Commun.* **14** 8240
[227] Tschirner T *et al* 2023 Saturation of the anomalous Hall effect at high magnetic fields in altermagnetic RuO_2 *APL Mater.* **11** 101103
[228] Gonzalez Betancourt R D *et al* 2023 Spontaneous anomalous Hall effect arising from an unconventional compensated magnetic phase in a semiconductor *Phys. Rev. Lett.* **130** 036702
[229] Takagi R *et al* 2024 Spontaneous Hall effect induced by collinear antiferromagnetic order at room temperature *Nat. Mater.* **24** 63–68
[230] Kluczyk K P *et al* 2024 Coexistence of anomalous Hall effect and weak magnetization in a nominally collinear antiferromagnet MnTe *Phys. Rev. B* **110** 155201
[231] Rial J *et al* 2024 Altermagnetic variants in thin films of Mn_5Si_3 *Phys. Rev. B* **110** L220411
[232] Reichlova H *et al* 2024 Observation of a spontaneous anomalous Hall response in the Mn_5Si_3 d-wave altermagnet candidate *Nat. Commun.* **15** 4961
[233] Leiviskä M *et al* 2024 Anisotropy of the anomalous Hall effect in thin films of the altermagnet candidate Mn_5Si_3 *Phys. Rev. B* **109** 224430
[234] Han L *et al* 2024 Electrical 180° switching of Néel vector in spin-splitting antiferromagnet *Sci. Adv.* **10** eadn0479
[235] Zhou Z, Cheng X, Hu M, Chu R, Bai H, Han L, Liu J, Pan F and Song C 2025 Manipulation of the altermagnetic order in CrSb via crystal symmetry *Nature* **638** 645–50
[236] Gray I, Deng Q, Tian Q, Chilcote M, Dodge J S, Brahlek M and Wu L 2024 Time-resolved magneto-optical effects in the altermagnet candidate MnTe *Appl. Phys. Lett.* **125** 212404
[237] Iguchi S, Kobayashi H, Ikemoto Y, Furukawa T, Itoh H, Iwai S, Moriwaki T and Sasaki T 2025 Magneto-optical spectra of an organic antiferromagnet as a candidate for an altermagnet *Phys. Rev. Res.* **7** 033026
[238] Shao D F, Zhang S H, Li M, Eom C B and Tsymbal E Y 2021 Spin-neutral currents for spintronics *Nat. Commun.* **12** 7061
[239] Samanta K, Jiang Y-Y, Paudel T R, Shao D-F and Tsymbal E Y 2024 Tunneling magnetoresistance in magnetic tunnel junctions with a single ferromagnetic electrode *Phys. Rev. B* **109** 174407
[240] Noh S *et al* 2025 Tunneling magnetoresistance in altermagnetic RuO_2-Based magnetic tunnel junctions *Phys. Rev. Lett.* **134** 246703

[241] Liu Q, Kang J, Wang P, Gao W, Qi Y, Zhao J and Jiang X 2024 Inverse magnetocaloric effect in altermagnetic 2D Non-van der Waals FeX (X = S and Se) semiconductors *Adv. Funct. Mater.* **34** 2402080
[242] Han L *et al* 2025 Nonvolatile anomalous Nernst effect in Mn_5Si_3 with a collinear Néel vector *Phys. Rev. Appl.* **23** 044066
[243] Badura A *et al* 2025 Observation of the anomalous Nernst effect in altermagnetic candidate Mn_5Si_3 *Nat. Commun.* **16** 7111
[244] Sürgers C, Fischer G, Campos W H, Hellenes A B, Šmejkal L, Sinova J, Merz M, Wolf T and Wernsdorfer W 2024 Anomalous Nernst effect in the noncollinear antiferromagnet Mn_5Si_3 *Commun. Mater.* **5** 176
[245] Li W, Xu C, Wang M, Zou M, Li W, Wang H, Jiang W and Wang B 2025 Large anomalous Nernst effect in a metallic altermagnet CrSb single crystal *Phys. Rev. B* **112** L100401
[246] Liu Z, Ozeki M, Asai S, Itoh S and Masuda T 2024 Chiral split magnon in altermagnetic MnTe *Phys. Rev. Lett.* **133** 156702
[247] Leenders R A, Afanasiev D, Kimel A V and Mikhaylovskiy R V 2024 Canted spin order as a platform for ultrafast conversion of magnons *Nature* **630** 335–9
[248] Zhang Z *et al* 2024 Terahertz field-induced nonlinear coupling of two magnon modes in an antiferromagnet *Nat. Phys.* **20** 801–6
[249] Zhang Z *et al* 2024 Terahertz-field-driven magnon upconversion in an antiferromagnet *Nat. Phys.* **20** 788–93
[250] Sun Q, Guo J, Wang D, Abernathy D L, Tian W and Li C 2025 Observation of chiral magnon band splitting in altermagnetic hematite *Phys. Rev. Lett.* **135** 186703
[251] Zhu W, Bai H, Han L, Pan F and Song C 2025 Tunable quantum anomalous Hall effect via crystal order in spin-splitting antiferromagnets *Nano Lett.* **25** 5672–8
[252] Šmejkal L 2024 Altermagnetic multiferroics and altermagnetoelectric effect (arXiv:2411.19928)
[253] Gu M, Liu Y, Zhu H, Yananose K, Chen X, Hu Y, Stroppa A and Liu Q 2025 Ferroelectric switchable altermagnetism *Phys. Rev. Lett.* **134** 106802
[254] Zhang K, Feng Y, Chen Y, Gong J, Xu L, Wu Z, Liu C, Chen C, Shimada K and Qiao L 2025 Spin-momentum locking in locally noncentrosymmetric quantum materials *Rep. Prog. Phys.* **88** 106503
[255] Jungwirth T *et al* 2025 Symmetry, microscopy and spectroscopy signatures of altermagnetism (arXiv:2506.22860)
[256] Baltz V, Manchon A, Tsoi M, Moriyama T, Ono T and Tserkovnyak Y 2018 Antiferromagnetic spintronics *Rev. Mod. Phys.* **90** 015005
[257] 2026 An alternate chapter in magnetism *Nat. Phys.* **22** 1
[258] Wu C, Sun K, Fradkin E and Zhang S-C 2007 Fermi liquid instabilities in the spin channel *Phys. Rev. B* **75** 115103
[259] Wu C and Zhang S-C 2004 Dynamic generation of spin-orbit coupling *Phys. Rev. Lett.* **93** 036403
[260] Zhu C, Pilch P, Reinold A, Kudlacik D, Springholz G, Bonanni A, Assmann M, Cinchetti M and Wang Z 2023 Ultrafast dynamics of optically excited charge carriers in the room-temperature antiferromagnetic semiconductor $\alpha-$MnTe *Phys. Rev. Mater.* **7** 054601
[261] Linder J and Robinson J W A 2015 Superconducting spintronics *Nat. Phys.* **11** 307–15
[262] Han J, Yoon J-Y, Ohno H and Fukami S 2025 Unconventional responses in non-collinear antiferromagnets *Newton* **1** 100012
[263] Rimmler B H, Pal B and Parkin S S P 2025 Non-collinear antiferromagnetic spintronics *Nat. Rev. Mater.* **10** 109–27
[264] Yu Y, Lyngby M B, Shishidou T, Roig M, Kreisel A, Weinert M, Andersen B M and Agterberg D F 2025 Odd-parity magnetism driven by antiferromagnetic exchange *Phys. Rev. Lett.* **135** 046701
[265] Luo X-J, Hu J-X and Law K 2025 Spin symmetry criteria for odd-parity magnets (arXiv:2510.05512)
[266] Nakatsuji S, Kiyohara N and Higo T 2015 Large anomalous Hall effect in a non-collinear antiferromagnet at room temperature *Nature* **527** 212–5
[267] Chen H, Niu Q and MacDonald A H 2014 Anomalous Hall effect arising from noncollinear antiferromagnetism *Phys. Rev. Lett.* **112** 017205
[268] Birk Hellenes A *et al* 2023 P-wave magnets (arXiv:2309.01607)
[269] Chakraborty A, Birk Hellenes A, Jaeschke-Ubiergo R, Jungwirth T, Šmejkal L and Sinova J 2025 Highly efficient non-relativistic Edelstein effect in nodal p-wave magnets *Nat. Commun.* **16** 7270
[270] Luo X-J, Hu J-X, Hu M-L and Law K T 2025 Spin group symmetry criteria for odd-parity magnets (arXiv:2510.05512)
[271] Sarkar R 2025 Altermagnet with a metallic touch *Nat. Phys.* **21** 691–2
[272] Attias L, Levchenko A and Khodas M 2024 Intrinsic anomalous Hall effect in altermagnets *Phys. Rev. B* **110** 094425
[273] Phillips C, Pokharel G, Shtefiienko K, Bhandari S R, Graf D E, Rai D P and Shrestha K 2025 Electronic structure of the altermagnet candidate $FeSb_2$: high-field torque magnetometry and density functional theory studies *Phys. Rev. B* **111** 075141
[274] Regmi R B *et al* 2025 Altermagnetism in the layered intercalated transition metal dichalcogenide $CoNb_4Se_8$ *Nat. Commun.* **16** 4399
[275] Sakhya A P *et al* 2025 Electronic structure of a layered altermagnetic compound $CoNb_4Se_8$ (arXiv:2503.16670)
[276] Dale N *et al* 2024 Non-relativistic spin splitting above and below the Fermi level in a g-wave altermagnet (arXiv:2411.18761)
[277] Sah A *et al* 2025 Altermagnetism, Kagome flat band, and Weyl fermion states in magnetically intercalated transition metal dichalcogenides (arXiv:2510.21968)
[278] Fernandes R M, de Carvalho V S, Birol T and Pereira R G 2024 Topological transition from nodal to nodeless Zeeman splitting in altermagnets *Phys. Rev. B* **109** 024404
[279] López-Moreno S, Romero A H, Mejía-López J, Muñoz A and Roshchin I V 2012 First-principles study of electronic, vibrational, elastic, and magnetic properties of FeF${}_{2}$ as a function of pressure *Phys. Rev. B* **85** 134110
[280] Vistoli L *et al* 2019 Giant topological Hall effect in correlated oxide thin films *Nat. Phys.* **15** 67–72
[281] Noda Y, Ohno K and Nakamura S 2016 Momentum-dependent band spin splitting in semiconducting MnO_2: a density functional calculation *Phys. Chem. Chem. Phys.* **18** 13294–303
[282] Guo P-J, Gu Y, Gao Z-F and Lu Z-Y 2023 Altermagnetic ferroelectric $LiFe_2F_6$ and spin-triplet excitonic insulator phase (arXiv:2312.13911)
[283] Milivojević M, Orozović M, Picozzi S, Gmitra M and Stavrić S 2024 Interplay of altermagnetism and weak ferromagnetism in two-dimensional RuF_4 *2D Mater.* **11** 035025
[284] Naka M, Hayami S, Kusunose H, Yanagi Y, Motome Y and Seo H 2020 Anomalous Hall effect in κ-type organic antiferromagnets *Phys. Rev. B* **102** 075112
[285] Chen H *et al* 2025 Spin-splitting magnetoresistance in altermagnetic RuO_2 thin films *Adv. Mater.* **37** e2507764
[286] Pawula F, Fakih A, Daou R, Hébert S, Mordvinova N, Lebedev O, Pelloquin D and Maignan A 2024 Multiband transport in RuO_2 *Phys. Rev. B* **110** 064432
[287] Rai B, Patra K, Bera S, Kalimuddin S, Deb K, Mondal M, Mahadevan P and Kumar N 2025 Direction-dependent conduction polarity in altermagnetic CrSb *Adv. Sci.* **12** e2502226

[288] Occhialini C A, Bisogni V, You H, Barbour A, Jarrige I, Mitchell J F, Comin R and Pelliciari J 2021 Local electronic structure of rutile RuO_2 *Phys. Rev. Res.* **3** 033214
[289] Tsirlin A A, Uykur E and Janson O 2025 Is ruthenium dioxide altermagnet? (arXiv:2511.01647)
[290] Choi I H, Jeong S G, Jalan B and Lee J S 2026 Exploring altermagnetism in RuO_2: from conflicting experiments to emerging consensus *Nano Convergence* **13** 1
[291] Kunitomi N, Hamaguchi Y and Anzai S 1964 Neutron diffraction study on manganese telluride *J. Phys. France* **25** 568–74
[292] Giebultowicz T M, Klosowski P, Samarth N, Luo H, Furdyna J K and Rhyne J J 1993 Neutron-diffraction studies of zinc-blende MnTe epitaxial films and MnTe/ZnTe superlattices: the effect of strain and dilution on a strongly frustrated fcc antiferromagnet *Phys. Rev. B* **48** 12817–33
[293] Kriegner D *et al* 2016 Multiple-stable anisotropic magnetoresistance memory in antiferromagnetic MnTe *Nat. Commun.* **7** 11623
[294] Zhou L-J *et al* 2026 Surface-state-driven anomalous Hall effect in altermagnetic MnTe films (arXiv:2602.09363)
[295] Chen Ye C, Tenzin K, Sławińska J and Autieri C 2026 Dominant orbital magnetization in the prototypical altermagnet MnTe *Phys. Rev. B* **113** 014413
[296] Belashchenko K D 2025 Giant strain-induced spin splitting effect in MnTe, a g-wave altermagnetic semiconductor *Phys. Rev. Lett.* **134** 086701
[297] Xie Z *et al* 2014 Orbital-selective spin texture and its manipulation in a topological insulator *Nat. Commun.* **5** 3382
[298] Cai Y *et al* 2025 Observation of highly spin-polarized dangling bond surface states in rare-earth pnictide tellurides *Adv. Mater.* **37** 2411733
[299] Zhang K *et al* 2021 Observation of spin-momentum-layer locking in a centrosymmetric crystal *Phys. Rev. Lett.* **127** 126402
[300] Wang M-X *et al* 2012 The coexistence of superconductivity and topological order in the $Bi2Se_3$ thin films *Science* **336** 52–55
[301] Novoselov K S, Geim A K, Morozov S V, Jiang D, Zhang Y, Dubonos S V, Grigorieva I V and Firsov A A 2004 Electric field effect in atomically thin carbon films *Science* **306** 666–9
[302] Li J, Zhang R-X, Yin Z, Zhang J, Watanabe K, Taniguchi T, Liu C and Zhu J 2018 A valley valve and electron beam splitter *Science* **362** 1149–52
[303] Zhao C *et al* 2020 Strain tunable semimetal–topological-insulator transition in monolayer 1T’-WTe2 *Phys. Rev. Lett.* **125** 046801
[304] Cao Y, Fatemi V, Fang S, Watanabe K, Taniguchi T, Kaxiras E and Jarillo-herrero P 2018 Unconventional superconductivity in magic-angle graphene superlattices *Nature* **556** 43–50